의학박사 학위논문

Mechanistic Physiologically based Pharmacokinetic and Pharmacokinetic/Pharmacodynamic Models to Evaluate the Mutual Relationships between an Acid Pump Antagonist and Intragastric pH in Humans

−Using YH4808, a novel K^+−competitive acid blocker, as an example−

위산 펌프 길항제와 위 내 산도 상호간의 효능 관계를 규명하기 위한 생리학적 약물 동태 모델과 약동/약력학 모델 구축 연구

−칼륨 경쟁적 위산 분비 억제제인 YH4808 을 예시로−

2019 년 8 월

서울대학교 융합과학기술대학원

방사선융합의생명 전공

이 현 아

A thesis of the degree of Doctor of Philosophy

위산 펌프 길항제와 위 내 산도 상호간의 효능 관계를 규명하기 위한 생리학적 약물 동태 모델과 약동/약력학 모델 구축 연구

-칼륨 경쟁적 위산 분비 억제제인 YH4808 을 예시로-

Mechanistic Physiologically based Pharmacokinetic and Pharmacokinetic/Pharmacodynamic Models to Evaluate the Mutual Relationships between an Acid Pump Antagonist and Intragastric pH in Humans

-Using YH4808, a novel K^+-competitive acid blocker, as an example-

August 2019

Biomedical Radiation Sciences

Graduate School of Convergence Science and Technology

Seoul National University

Hyun A Lee

위산 펌프 길항제와 위 내 산도 상호간의 효능 관계를 규명하기 위한 생리학적 약물 동태 모델과 약동/약력학 모델 구축 연구

– 칼륨 경쟁적 위산 분비 억제제인 YH4808을 예시로–

지도교수 이 형 기

이 논문을 의학박사 학위논문으로 제출함

2019년 8월

서울대학교 융합과학기술대학원

방사선융합의생명 전공

이 현 아

이 현 아 의 의학박사 학위논문을 인준함

2019년 8월

위 원 장 _____ (인)

부위원장 _____ (인)

위 원 _____ (인)

위 원 _____ (인)

위 원 _____ (인)

Mechanistic Physiologically based Pharmacokinetic and Pharmacokinetic/Pharmacodynamic Models to Evaluate the Mutual Relationships between an Acid Pump Antagonist and Intragastric pH in Humans

−Using YH4808, a novel K^+−competitive acid blocker, as an example−

by
Hyun A Lee

A thesis submitted to the Biomedical Radiation Sciences in partial fulfillment of the requirements for the degree of Doctor of Philosophy in Medicine at Seoul National University Graduate School of Convergence Science and Technology

August 2019

Approved by the Thesis Committee:

Professor _____Chairman

Professor _____Vice chairman

Professor _____

Professor _____

Professor _____

ABSTRACT

Mechanistic Physiologically based Pharmacokinetic and Pharmacokinetic/Pharmacodynamic Models to Evaluate the Mutual Relationships between an Acid Pump Antagonist and Intragastric pH in Humans

– Using YH4808, a novel K^+–competitive acid blocker, as an example–

Hyun A Lee

Biomedical Radiation Sciences

Graduate School of Convergence Science and Technology

Seoul National University

Introduction: YH4808 is a highly potent, selective and reversible potassium–competitive acid blocker of the H+/K+–ATPase under clinical development to treat gastric acid–related diseases. The pharmacokinetics of YH4808 was dose–proportional in humans after a single oral dose at 30–800 mg. However, the systemic exposure to YH4808 decreased after multiple oral administrations, particularly at higher doses (200 and 400 mg). The reduced solubility of YH4808 caused by

elevated intragastric pH after treatment with YH4808 was suggested as the main cause of the reduced exposure. In this study, first, a physiologically-based pharmacokinetic (PBPK) model was developed to predict the pharmacokinetic (PK) profiles of YH4808 after single and multiple administration and investigate the mechanistic basis of the decreased exposure of YH4808 after repeated oral administration at higher doses using the developed human PBPK model. Second, we developed a pharmacokinetic and pharmacodynamics (PK/PD) model to quantitatively evaluated the mutual relationships between the plasma concentrations of YH4808 and the time course of intragastric pH after single and multiple oral administration in humans.

Methods: A PBPK model was developed using the physicochemical data, *in vitro* preclinical and clinical data of YH4808, which was further refined using human plasma concentrations obtained from a single-dose ascending phase I clinical trial of YH4808 with the SimCYP (Certara USA, Inc., Princeton, USA). Compartments were included for the brain, heart, lung, kidney, muscle, spleen, liver, gastrointestinal (GI) tract, pancreas, and a combined compartment for the remaining

tissues. All compartments except the GI tract and liver were assumed to be well-stirred and their clearances were limited by blood flow. The absorption of YH4808 was described by the advanced dissolution, absorption and metabolism (ADAM) model implemented in SimCYP®, which divides the GI tract into nine segments, assuming permeability-limited disposition in the GI tract and liver. Biliary route is the major elimination pathway of YH4808, and the clearance was estimated using in vitro hepatic microsomal intrinsic clearance data.

A PK/PD model was developed simultaneously using pooled data of the plasma concentrations of YH4808 and intragastric pH profiles obtained from healthy subjects who received a single (30-800 mg) or multiple (100-400 mg) oral doses or their matching placebos (intragastric pH only). The modeling was conducted using the first-order conditional estimation with interaction (FOCE-I) method implemented in NONMEM version 7.3 (ICON Development Solutions, Ellicott City, MD, USA). The effects of covariates (i.e., age, body weight and height) were also evaluated and tested. The final model was qualified based on the precision of parameter estimates, diagnostic plots and visual predictive check plots.

Results: In PBPK modeling study, the PK profiles of YH4808 in human after multiple oral administrations (100, 200 and 400 mg) were predicted using a refined PBPK model, and the PBPK model adequately predicted the observed concentrations at 100 mg dosing. However, the model failed to predict a decreased exposure after multiple oral administrations at higher doses of 200 and 400 mg. The reduced solubility of YH4808 at higher pH was hypothesized as the main cause of the reduction in exposure such that absorption was decrease as pH was increased. It was confirmed by PBPK modeling and simulation, where intragastric pH was increased by YH4808.

In PK/PD modeling study, a two-compartment PK model with lagged first-order absorption model and a sigmoid maximum effect model linked with an effect compartment best described the observed YH4808 plasma concentrations and intragastric pH profiles over 24-hour period after YH4808 dosing, respectively. To address changes in intragastric pH over time affecting the plasma concentration of YH4808, we introduced a feedback path such that increased intragastric pH decreases the relative bioavailability of YH4808.

Conclusion: A PBPK model adequately predicted observed concentrations of YH4808 after single and multiple administration in human, and a simulation experiment based on the human PBPK model indicated that the pH-dependent solubility of YH4808 could have resulted in the reduced exposure after multiple administration. A PK/PD model also adequately described quantitatively mutual relationships between the plasma concentrations of YH4808 and the time course of intragastric pH after single and multiple administration in humans. Our analysis provides mechanistic insight into relationship between the exposure to YH4808 and intragastric pH, which allow for devising optimal dosing regimens for YH4808.

* A part of this work is published in the European Journal of Pharmaceutical Sciences (Lee HA, Lee KR, Jang SB, Chung SY, Yu KS, Lee H. A physiologically-based pharmacokinetic model adequately predicted the human pharmacokinetic profiles of YH4808, a novel K+-competitive acid blocker. Eur J Pharm Sci. 2019 Mar 15;130:1-10)

Keywords: intragastric pH, physiologically-based pharmacokinetics, pharmacokinetics, pharmacodynamics, modeling, simulation, potassium-competitive acid blocker

Student number: 2015-30724

CONTENTS

LIST OF TABLES

LIST OF FIGURES

LIST OF ABBREVIATIONS

Add Error	Additive error
AUC	Area under the concentration−time curve
Ce	Concentration of YH4808 in the effect compartment
CI	Confidence interval
C_{max}	Maximum plasma concentration
CL/F	Apparent clearance
CV	Coefficient of variation
DDI	Drug−drug interaction
EC_{50}	Plasma (or effect site) concentration needed to half of E_{max}
E_{max}	Maximum effect
FOCE INTER	First−order conditional estimation with interaction
h	hour(s)
HPLC	High performance liquid chromatography
H. pylori	*Helicobacter pylori*
IRB	Institutional Review Board
IIV	Inter−individual variability
Ka	Absorption rate constant

LC-MS/MS	Liquid chromatography-tandem mass spectrometer
NA	Not applicable
NONMEM	Non-linear mixed effect model
OFV	Objective function value
P-CAB	Potassium-competitive acid blocker
PD	Pharmacodynamic, pharmacodynamics
PK	Pharmacokinetic, pharmacokinetics
PPI	Proton pump inhibitor
Prop Error	Proportional error
Q	Inter-compartmental clearance
QD	Once a day
RSE	Relative standard error
RV	Residual variability
SD	Standard deviation
T_{max}	Time to peak plasma concentration
$t_{1/2}$	Terminal elimination half-life
V_C	Central volume of distribution
V_P	Peripheral volume of distribution
WT	Body weight

INTRODUCTION

The potassium-competitive acid blocker (P-CAB) and proton pump inhibitors (PPIs) are potent acid-reducing agents (ARAs) to treat patients with gastroesophageal reflux disease, peptic ulcer disease, and other acid-related diseases. P-CABs inhibit the activity of the gastric H^+/K^+-ATPase by reversible K^+-competitive ionic binding to the enzyme, leading to reduced H^+ transport into the parietal cell canaliculus in exchange for K^+ [1,2]. Unlike PPIs such as omeprazole, rabeprazole, and lansoprazole, P-CABs do not require prior proton pump activation to achieve antisecretory effect [3]. Furthermore, the inhibition of acid secretion by the P-CAB is fast because it rapidly reaches the peak plasma concentration after oral administration [4]. For example, BY841, a P-CAB, reached the peak serum concentrations 0.5-1.5 hours post-dose [5]. Likewise, revaprazan,(i.e.,YH1885) another P-CAB, achieved the peak plasma concentrations within 1.3-2.5 hours after a single oral dose [6]. Additionally, the clinical utility of PPIs has been limited due to their large inter-subject variability, partly attributed to the genetic polymorphisms in the cytochrome P450 (CYP) isozymes, particularly CYP2C19, that metabolize

PPIs in the liver (except for tenatoprazole)[7]. Because of the sensitivity of PPIs to CYP2C19, the pharmacokinetic (PK) profiles of PPIs could vary largely between extensive, intermediate, and poor metabolizers [8]. Therefore, P-CABs may offer additional therapeutic advantages including a faster onset of action and greater and prolonged efficacy over the entire dosing interval than PPIs [9].

YH4808(2-(1-Allyl-2,3-dimethyl-1H-pyrrolo[2,3-c]pyridine-7-yl)-1,2,3,4-tetrahydroisoquinoline hydrochloride) is a novel, selective and reversible P-CAB under clinical development to treat gastroesophageal reflux disease and peptic ulcer disease (Yuhan Corporation, South Korea)[10]. YH4808 is a highly potent and selective H^+, K^+-ATPase inhibitor compared with other reference compounds including esomeprazole [10]. Because YH4808 is rapidly absorbed and does not require an acidic environment for activation or protonation, YH4808 can immediately bind to the H^+/K^+-ATPase inhibitor, which leads to fast and marked inhibition of gastric acid secretion compared with esomeprazole, a PPI. To support this notion, the half maximal inhibitory concentration (IC_{50}) of YH4808 for H^+/K^+-ATPase was almost 1,000 times lower than that of esomeprazole (3.4 vs. 3365

nM).[11] YH4808 is extensively distributed in the gastric tissue after oral administration [11]. In addition, YH4808 is metabolized by various CYP isozymes, which makes the PK and pharmacodynamics (PD) of YH4808 less dependent on CYP2C19, which is genetically polymorphic [10]. M3 and M8 were identified as the major metabolites of YH4808 *in vitro* and *in vivo* across the various species including humans although the major pharmacologic activity appeared to arise from the parent drug [10]. YH4808 did not significantly inhibit or induce CYP450 isozymes including CYP1A2, 2A6, 2B6, 2C8, 2C9, 2C19, 2D6 and 3A4 in human hepatic microsomes, suggesting little potential for drug-drug interactions (DDIs) (in-house data). In a previous clinical study, after YH4808 100-400 mg had been administered for 7 days, YH4808 maintained intragastric pH >4 for approximately 70% of a 24-hours time period. Although YH4808 exhibited a dose-proportional PK profiles at a single dose of 30-800 mg, the systemic exposure of YH4808 decreased after multiple oral administrations, particularly at higher doses (200 and 400 mg) [10]. The reduced solubility of YH4808 by elevated pH after multiple administrations was hypothesized as the main cause of the reduction in exposure.

Modeling and simulation have the potential to be important tools in all phases of new drug development from preclinical to clinical and post-marketing phases, providing scientific evidence upon which to base crucial decisions during all stages of a drug product's life cycle. Modeling and simulation use of mathematical and statistical models that are essentially simplified descriptions of complex systems under investigation. One approach to such models is a "bottom-up" or physiologically-based pharmacokinetic (PBPK) approach, with models comprising equations and parameters that try to more closely reproduce underlying anatomic distributions and physiologic functions [12]. Recently, recognition of the value of PBPK modeling and simulation in predicting human PK was growing, especially regarding DDI risk. PBPK modeling analysis can simulate the PK profiles of a compound not only in the plasma, but also in other organs and tissues by integrating drug-specific (i.e., the absorption, distribution, metabolism, and excretion (ADME) and physicochemical properties of a compound) and system-specific information (e.g., human physiology, demographics, and heterogeneity)[13-15]. This PBPK modeling analysis (i.e., "bottom-up" approach) has been recently used in the clinical development to evaluate how

food, formulation and acid reducing agents (ARAs) impact drug absorption [16,17]. Furthermore, when combined with PD models, a PBPK model can be also used to estimate the time course of drug response [15].

The alternative is the "top-down" system of empirical equations with relatively few parameters. Equations and estimation of the probability distribution of parameters are not chosen to faithfully reproduce underlying anatomy and physiology but to best reproduce the distribution of observed data. Model validation is based on bias, imprecision, and distribution of predictions relative to the original or to external, independent data. This is most often termed "population pharmacokinetic/pharmacodynamics (PK/PD) modeling" [18,19]. Population PK/PD modeling based on clinical PK and PD observation characterizes the impact of intrinsic and extrinsic factors (covariates) on the inter-individual variability (IIV) in PK parameters using compartmental and increasingly mechanistic models. Population PK/PD modeling also uses to link PK and PD in order to establish and evaluate dose-concentration-response relationships and subsequently describes and predicts the effect-time courses resulting from a drug dose [20]. In clinical drug development, PK/PD modeling

using data of phase I dose escalation studies on healthy subjects provides information for the rationale design of all subsequent clinical development phases, especially in identifying effective and safe dosage regimens before large clinical trials are started.

Especially, mechanism-based population PK/PD model quantitatively characterize specific processes on the causal path between drug administration and effect. Most mechanism-based population PK/PD models typically integrate PK (e.g., PBPK) reflecting the relevance physiology and disease, and the nature of drug-target interaction (i.e., pharmacology) (Figure 1). Mechanism-based PK/PD model constitutes a scientific basis for rational drug development.

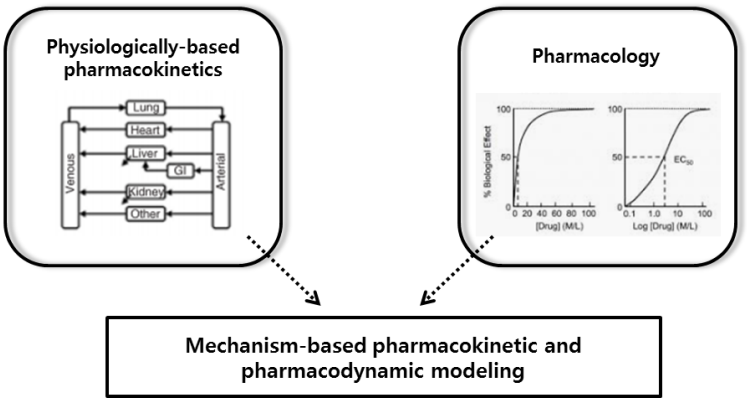

Figure 1. Major components contributing to assembly of mechanism-based pharmacokinetic/pharmacodynamic models

In the case of capecitabine, orally administered triple pro-drug of 5-fluorouracil that is approved for the treatment of breast and colorectal cancer, a mechanism-based PK/PD modeling combined with PBPK modeling approach used in a development to provide a more thorough understanding of what the key predictors of its PBPK activity are, and how variability in these predictors may affect its PK and PD, and ultimately, clinical outcomes [21]. The mechanism-based PK/PD model combined with PBPK modeling using clinical data were developed to characterize the activity of capecitabine and its metabolites, and the clinical outcomes under varying physiological conditions such as creatinine clearance or activity of key metabolic enzymes. The results of these modeling were consistent with capecitabine's rational design. In our study, we developed both PBPK and mechanism-based PK/PD model to confirm and evaluate the relationships between the plasma concentrations of YH4808 and the time course of intragastric pH after single and multiple oral administrations in humans. First, we developed the PBPK model to investigate why the systemic exposure decreases after multiple oral administration, and then the mechanism that explain the decrease exposure was applied to the PK/PD model. In other words, this study

provides a real-life case in clinical drug development, where both PK/PD ("top-down") and PBPK ("bottom-up") approaches are applied using all the available data (in vitro, nonclinical and clinical (healthy volunteers)) to elucidate how increased intragastric pH will impact the PK of YH4808.

Objectives

The main objectives of this study are 1) to develop a human PBPK model of YH4808 using its physicochemical properties and *in vitro* and *in vivo* pre-clinical data to predict the PK profiles of YH4808 in various clinical settings after single and multiple oral administrations for further clinical development, 2) to investigate the mechanistic basis of the decrease exposure to YH4808 after repeated oral administration at higher doses using the developed human PBPK model, and 3) to develop a mechanism-based PK/PD model to quantitatively evaluate the mutual relationships between the plasma concentrations of YH4808 and the time course of intragastric pH after single and multiple oral administration in humans.

METHODS

1. Physiologically-based pharmacokinetic (PBPK) modeling of YH4808

1.1 Materials

YH4808 (Figure 2) was synthesized at Yuhan Corporation, Seoul, South Korea. Oxybutynin (internal standard) was supplied by Sigma-Aldrich (St.Louis, MO, USA). Pooled human, rat and mouse microsomes were purchased from BD Gentest (Woburn, MA, USA), and dog and monkey microsomes were purchased from In vitro Technologies, Inc. (Melbourne, Australia). All the other reagents (acetonitrile, methanol, formic acid, and ammonium formate) were commercial products of analytical grade and used without further purification.

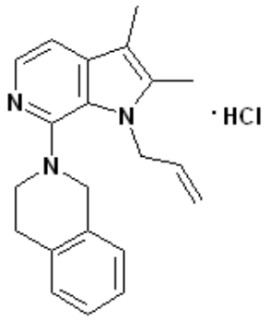

Figure 2. Chemical structure of YH4808

1.2. Caco-2 transcellular permeability

Human colon adenocarcinoma cells (Caco-2) were obtained from Korean Cell Line Bank (Seoul, South Korea). The cells were cultured for 21 days in 12 transwell under 95% air/5% CO_2, relative humidity of 90% and 37°C. On the experiment day, the integrity of the cell monolayer was evaluated by measuring the transepithelial electrical resistance (TEER) using a EVOM Epithelial Volt/ohm-meter (World Precision Instruments, FL, USA). The incubation medium was Hank's balanced salt solution containing 25 mM N-2-hydroxyethylpiperazine-N'-2-ethanesulfonic acid and 25 mM glucose at pH 7.4. The test compound solution was prepared by diluting 0.5% dimethyl sulfoxide (DMSO) stock solution (all tested at a final concentration of 0.1-10 μM). Incubations were started by placing the test compound at the apical side of the transwell for assessing the permeability in the A to B (apical to basolateral) direction and the incubation lasted 80 minutes in a 37°C incubator. Mannitol was used as the quality control of the given batch of the Caco-2 culture.

The apparent permeability coefficient (P_{app}) values were calculated as follows:

$$P_{app}(cm/sec) = \frac{dQ}{dt} \times \frac{1}{A \times C_0} \quad (1)$$

,where A, C_0 and dQ/dt represent the insert surface area (cm^2), initial donor drug concentration (μM) and the amount of drug transported within a given time period (μmol/sec), respectively.

1.3. Metabolic stability

Pooled microsomes from rat, mouse, dog, monkey and human liver were used for assays. Incubations (400 μL) consisted of liver microsomes (1 mg/mL), NADPH generating system (0.1 M glucose 6-phosphate, 1 unit glucose 6-phosphate dehydrogenase, 10 mg/mL β-$NADPH^+$) and 0.1 M potassium phosphate buffer (pH 7.4). Following pre-incubation (5 min, 37℃), reactions were initiated by spiking stock solutions of YH4808 (10 μM). Samples were taken at 0, 10, 20, 30, 45, 60, and 120 min and quenched with methanol. Then, the samples were centrifuged for 10 min at 3,000 rpm, and the supernatants (5 μL) were analyzed by LC-MS/MS. The metabolic half-life ($t_{1/2}$) was calculated based on the slope of the declining portion on the linear regression line for the natural logarithm-transformed remaining percentage of the substrate versus incubation time.

1.4. Inhibition of CYP enzymes by YH4808

The effect of YH4808 (0.1−50 μM) on the metabolism of substrates by corresponding selective CYP enzymes was investigated using pooled human liver microsomes (1 mg/mL). The following drugs were used as CYP substrates: 40 μM phenacetin (CYP1A2), 2.5 μM coumarin (CYP2A6), 10 μM paclitaxel (CYP2C8), 10 μM diclofenac (CYP2C9), 5 μM dextromethorphan (CYP2D6), and 2.5 μM midazolam (CYP3A)[22]. Individual substrates were pre−incubated with human liver microsomes in the presence of YH4808 for 5 min at 37℃ before the addition of an NADPH−generating solution. A cocktail of 6 probe substrates was incubated for 15 min at 37℃, and then the reactions were terminated by adding 40 μL of a stop solution consisting of acetonitrile and 10 μM chlorpropamide. In vitro high−throughput P450 cocktail inhibition assay was used 6 substrates simultaneously against 6 CYP isozymes, and the samples were analyzed using an LC−MS/MS system. Control incubations were performed using carrier vehicle only. The extent of enzyme inhibition was expressed as the percentage of remaining enzyme activity compared with the control (in the absence of inhibitor). The inhibition data were fit to an enzyme inhibition model using a

nonlinear least-squares regression analysis (WinNonlin 4.0, Pharsight, A Certara Company, Princeton, NJ, USA). IC_{50} were determined with each of the CYP substrates. Inhibition potential was classified into three categories: potent (IC_{50} < 1 μM), moderate (1 μM < IC_{50} < 10 μM), and no or weak inhibition (IC_{50} > 10 μM) [23].

1.5. Plasma protein binding

The protein binding of YH4808 was determined in rat, dog, monkey and human plasma at two concentrations (150 and 300 ng/mL). The protein binding ratio was determined using ultracentrifuge devices (Optima^{TM} LE-80K, SW 60 Ti, Beckman Coulter, Indianapolis, IN, USA). Pooled male Sprague Dawley rat plasma was obtained from Innovative Research, and pooled human male plasma was purchased from Biomedex Inc. (Spokane, WA, USA). Pooled male beagle dog plasma and pooled male Cynomolgus monkey plasma were obtained from Yuhan Research Institute. YH4808, prepared in methanol as stock solution (1,000 μg/mL), was diluted in plasma to achieve the target concentrations. All measurements were performed in triplicate. Plasma samples were incubated for 30 min at 37°C and ultracentrifuged at 406,484.7 g for 5 hours at 4°C. After

finishing ultracentrifugation, 0.05 mL supernatant was mixed with 150 μL internal standard (oxybutynin, 500 ng/mL in 100% acetonitrile). The mixture was vortex-mixed for 30 secs and then centrifuged at 13,000 rpm for 10 min. The supernatant (100 μL) after centrifugation was transferred to HPLC auto-sampler vials and 7 μL was injected into the LC-MS/MS system.

The percentage of unbound drugs was calculated as follows:

$$\%\ \text{unbound drugs} = \frac{Concentration\ unbound\ drugs}{Concentration\ unbound\ drugs + Concentration\ protein\ fractions} \times 100 \quad (2)$$

1.6. Human pharmacokinetic study

Clinical PK data of YH4808 after single and multiple oral administration was obtained in a previous study [10], which was performed using a randomized, double-blind, single and multiple ascending dose design in healthy male subjects, 20-45 years of age, with a body weight >50 kg, and within ±20% of ideal body weight. The doses of YH4808 were 50, 100, 200 and 400 mg in the single dose study, and 100, 200 and 400 mg once daily for 7 days in the multiple dose study. For the PK analysis, blood samples were collected pre-dose (0 hour), 0.25, 0.5, 0.75, 1, 1.5, 2, 3, 4, 6, 8, 12, 24, 36 and 48 hours post-dose,

on Day 1 and 7 (the multiple dose study only). The PK parameters were estimated using a non-compartmental method implemented in Phoenix 6.4 software (WinNonlin 6.4., Pharsight, A Certara Company, Princeton, NJ, USA).

1.7. PBPK modeling in humans

A human PBPK model was developed using the physicochemical data of YH4808 and human physiological data (Figure 3). The compound-specific physicochemical (i.e., molecular weight, Log P, pKa and pH-solubility profile) and in vitro (i.e., fraction unbound. Caco-2 permeability, metabolic stability and inhibition of CYP enzymes) of YH4808 were obtained from Investigator Brochure provided by Yuhan Corporation, Seoul, South Korea. The advanced dissolution, absorption, and metabolism (ADAM) module in the SimCYP® Simulator was used to account for intestinal permeability in humans. We simulated the PK profiles of YH4808 in humans using the final animal PBPK model complemented by human *in vitro* data of YH4808 including microsomal clearance, plasma free fraction, and Caco-2 cell permeability along with YH4808-specific physicochemical data (Table 1). Each simulation was performed using 100 virtual males (i.e., 10 trials x 10 subjects), who had a mean body

weight of 70 kg with age ranging from 21 to 38 years as in the clinical study [10]. The dose, dosing interval, and dosing duration of YH4808 in the simulation were identical to those used in the clinical study [10].

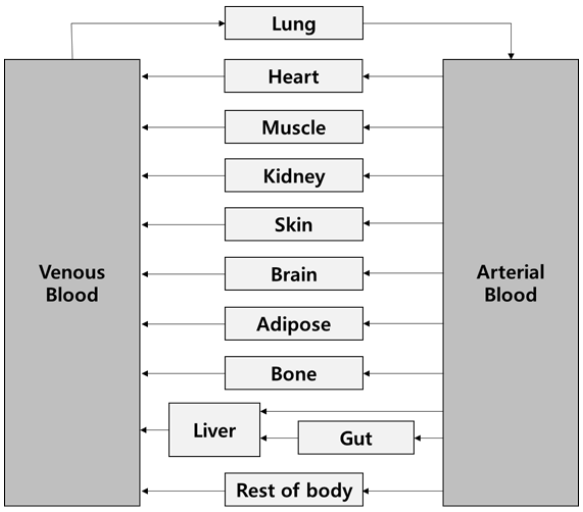

Figure 3. Schematic description of the physiologically-based pharmacokinetic model of YH4808

Table 1. Input parameters of a physiologically-based pharmacokinetic model for YH4808

	Input Value		Data Source
	Species	Human (50-90kg)	
Physicochemical property	Molecular weight (g/mol)	353.89	The nonclinical study of YH4808 for a new drug of GERD and PUD, Korea Health Industry Development Institute (2010)
	Log P	1.2	
	Compound type	Monoprotic base	
	pKa	6.995	
	pH-solubility profile	2.137 mg/mL at pH=2.0; 0.046 mg/mL at pH=6.0	
	Fraction unbound	0.0046	
Absorption	Absorption type	Advanced Dissolution, Absorption and Metabolism (ADAM) model	
	Caco-2 cell permeability (10^{-5} cm/s)	1.49	
Distribution	Distribution model	Full PBPK model	Prediction by SimCYP® simulator
	Tissue/plasma partition coefficient: Adipose	0.04	
	Tissue/plasma partition coefficient: Kidney	0.14	

			Brain	0.06		
			Liver	0.09		
			Gut	0.20		
	Prediction method			Rodgers et al. (Method 2)[a]		
Elimination	Elimination type	*In vivo* clearance		Enzyme kinetics		Investigator Brochure (Version 11.0) by Yuhan Corporation (2013)
			CYP2C19	V_{max}[b] (pmol/min/mg)	12.6	
				K_m (μM)[c]	68.6	
			CYP2D6	V_{max} (pmol/min/mg)	22.0	
				K_m (μM)	13.0	
Interaction	Inhibition constant (K_i, μM)[d]		CYP2C19	4.38		
			CYP2D6	1.71		

[a] Rodgers et al., (2005), J Pharm Sci 94(6):1259−1276, and Rodgers and Rowland (2006) J Pharm Sci 95(6):1238−1257
[b] V_{max}: Maximum rate of metabolite formation (pmol/min/mg protein)
[c] K_m: Michaelis−Menten constant (μM)
[d] K_i; Inhibition constant (μM)

1.8. Model optimization

We compared the PBPK model-predicted plasma concentration-time profiles of YH4808 with the observed ones in rats and dogs, which were further optimized by the Parameter Estimation module within the SimCYP® Simulator. The Parameter Estimation module adjusts estimated parameters such that they could better predict observed concentrations. Primarily, a least square objective function was fitted using the Nelder-Mead algorithm (Nelder and Mead, 1965). The expectation-maximization method was used to solve the maximum likelihood problem. Then, we further optimized the human PBPK model to adequately predict the concentration-time profiles of YH4808 in humans after a single oral administration at 50, 100, 200 and 400 mg. To this end, effective intestinal permeability (P_{eff}) values were estimated by the Nelder-Mead algorithm of the Parameter Estimation module in the SimCYP® Simulator. Finally, the optimized human PBPK model was used to predict the PK profiles of YH4808 after repeated once-daily oral administration at 100, 200 and 400 mg.

1.9. Model validation (drug–drug interactions, DDIs)

To validate the human PBPK model for YH4808, we simulated DDIs using the developed human PBPK model. For simulations of DDIs, the total clearance of YH4808 was primarily defined by the metabolic clearance. The metabolic clearance was defined by enzyme kinetic parameters, the maximum rate of metabolite formation (V_{max}) and the Michaelis–Menten constant (K_m) values, determined from the formation rate of metabolite CYP2C19 and CYP2D6 recombinant system (Table 1). V_{max} and K_m values were determined by nonlinear fitting using GraphPad Prism (La Jolla, CA, USA). The input inhibition constants (K_i) for CYP2C19 and CYP2D6 of YH4808 were obtained from experimental *in vitro* data (Table 1). The human PBPK model was utilized to simulate changes in the PK profile (AUC) of YH4808, substrate, in the presence of a strong CYP2C19 and CYP2D6 inhibitor (fluvoxamine for CYP2C19, fluoxetine for CYP2D6). Compound files for fluvoxamine 50 mg once daily and fluoxetine 40 mg once daily were used as provided in the SimCYP® Simulator. The predictive performance of DDIs using the human PBPK model of YH4808 was determined by calculating the ratio of model predicted exposure changes in substrate (AUC_{ratio}) [27]. Predicted AUC_{ratio} was defined as

$AUC_{with\ inhibitor}/AUC_{without\ inhibitor}$. The ratio of YH4808 AUC in the presence of an inhibitor (fluvoxamine and fluoxetine) to YH4808 AUC in the absence of an inhibitor was used as a measurement of magnitude of interaction.

1.10. Evaluation of model performance

We assessed the adequacy of the PBPK model first by visually comparing the model-predicted and observed concentration-time profiles of YH4808. Then, a ratio of the model-predicted to observed mean values was calculated for the PK parameter of YH4808 such as the area under the plasma concentration-time curve (AUC) from time 0 to the last observable concentration (AUC_{0-t}), AUC from time 0 to infinity (AUC_{inf}), AUC over dosing interval (AUC_{τ}), the peak concentration (C_{max}), and time to reach C_{max} (T_{max}). We concluded that the PBPK model performed adequately when a ratio of the model-predicted to observed mean values was contained within 0.5-2.0 [28,29].

2. Mechanism-based pharmacokinetic and pharmacodynamics (PK/PD) modeling of YH4808

2.1. Study design and subjects

The plasma concentration and intragastric pH data of YH4808 were derived from a phase I study conducted at the Clinical Trials Center in SNUH from 2009 to 2011.

Study design

This was a randomized, double-blind, placebo- and active comparator-controlled clinical study performed in two parts: a single ascending dose study (30, 50, 100, 200, 400, 600 and 800 mg), and a multiple ascending dose study (100, 200 and 400 mg once daily for 7 days). After an overnight fast, eligible subjects randomly received a single oral dose or multiple oral daily doses of YH4808 at the assigned dose, or placebo. 24-hours continuous, ambulatory intragastric pH monitoring on Day -1 (baseline), and Day 1 in the single dose study; on Day -1, Day 1, and Day 7 in the YH4808 100 mg and the 400 mg groups

in the multiple dose study. The YH4808 200 mg group in the multiple dose study received intragastric pH monitoring only on Day −1 and Day 7.

Subjects

Healthy male subjects aged 20 − 45 years with a body weight of >50 kg and within ±20% of ideal body weight were enrolled in this study provided that they presented no abnormalities based on medical history, physical examination, 12−lead electrocardiogram, serology (HBsAg, anti−HCV and anti−HIV antibody), clinical laboratory tests (chemistry, haematology and urinalysis), and urine drug screening. In the single dose study, subjects who were both positive and negative for *Helicobacter pylori* (*H. pylori*) were enrolled to explore the effects of YH4808 on intragastric pH profiles in the presence and absence of *H. pylori* infections. However, in the multiple dose study, *H. pylori*−negative subjects were only enrolled to avoid the effect of *H. pylori* infections on intragastric pH. Written informed consent was obtained before any study−related procedure was performed. This study was approved by the Institutional Review Board at SNUH, Seoul, South Korea, and was conducted in accordance with the principles of the Declaration of Helsinki

and Good Clinical Practice (clinicaltrials.gov registration number: NCT01007019).

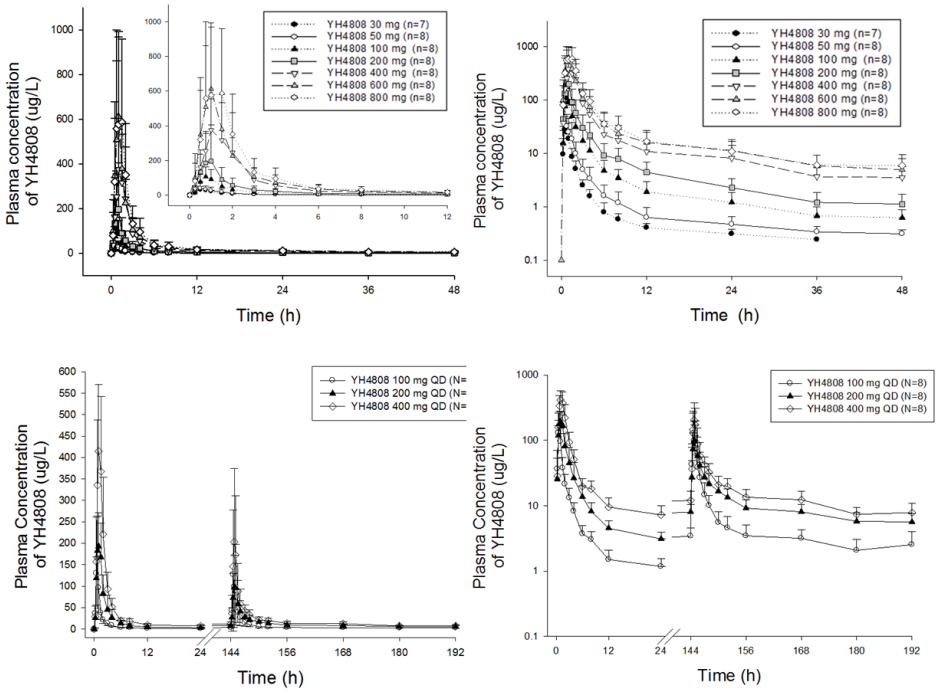

Figure 4. Mean plasma concentration–time profiles of YH4808 (left: linear scale; right: semi–log scale). Data presented as mean±standard deviation.
30–800 mg single doses of YH4808 under fasted conditions (top); multiple dose of 100–400 mg QD (once daily) for 7 days (bottom)

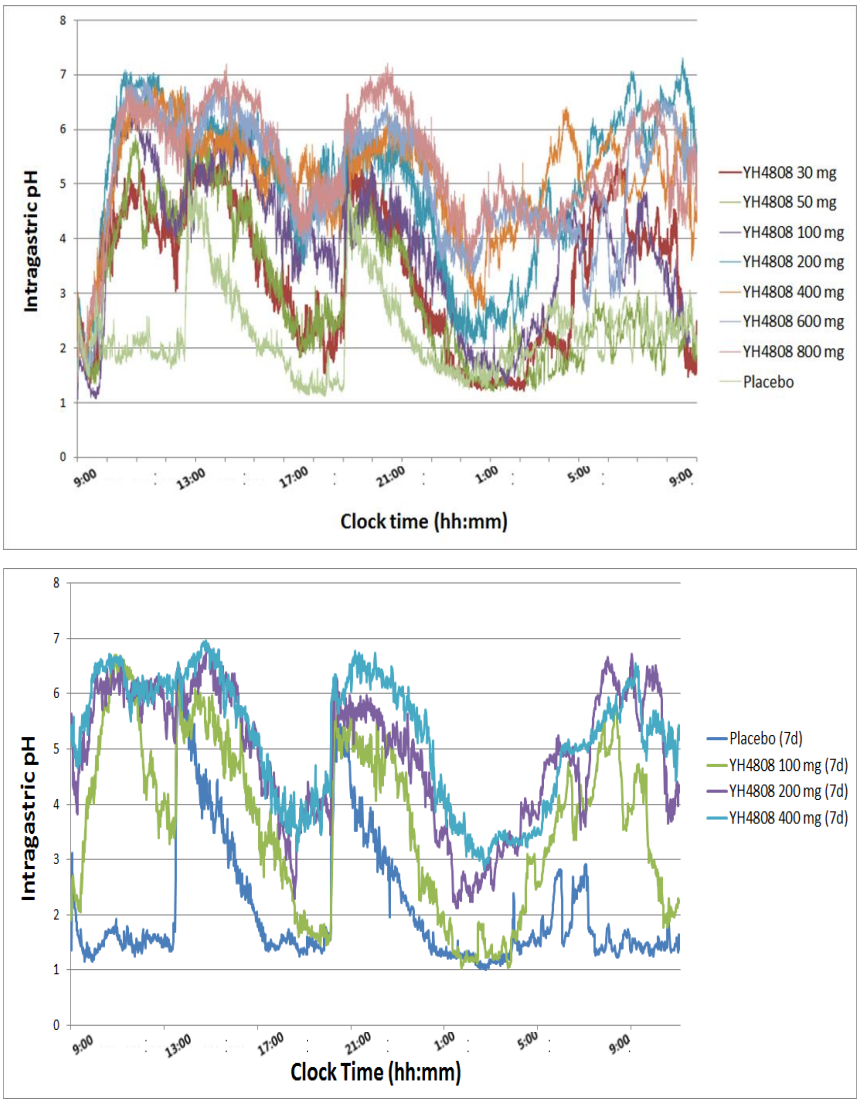

Figure 5. Mean 24 hr intragastric pH vs. time profiles of YH4808.
30-800 mg single doses of YH4808 (top); multiple dose of 100-400 mg at 7 day (bottom)

2.2. Population pharmacokinetic/pharmacodynamic model development

The plasma concentrations of YH4808 and intragastric pH profiles obtained from healthy subjects who received a single (30–800 mg) or multiple (100–400 mg) oral doses or their matching placebos (intragastric pH only) were pooled for a PK/PD analysis. A population PK/PD analysis was simultaneously performed using the first-order conditional estimation (FOCE) with interaction method implemented in NONMEM® version 7.3 (ICON Development Solutions, Ellicott City, MD, USA). For graphical visualization, RStudio (Version 1.0.153, The R Foundation for Statistical Computing, Vienna, Austria) was used. Model selection was based on the difference in objective function value (OFV), the graphical analysis of goodness-of-fit plot, and the relative standard error reflecting the precision of the parameter estimates.

Pharmacokinetic model development

Following visual assessment of the concentration-time profiles of YH4808 in phase I study (Figure 4), a 2-compartment disposition model with first-order absorption was evaluated as

the structural PK model for this analysis. To describe the rapid increase in plasma concentrations of YH4808, the model including lag time (ALAG1) was evaluate as well. The disposition kinetics were parameterized in terms of apparent clearance (CL, L/h), apparent volume of distribution (V_2 for central, and V_3 for peripheral volume, L), intercompartmental clearance (Q, L/h), and absorption rate constant (Ka, 1/h) using ADVAN13 and the first-order conditional estimation method with interaction (FOCE-I). The inter-individual variability (IIV) of the PK parameters was evaluated using an exponential error model, and the residual variability (RV) was evaluated using a combined proportional and additive random effects model. Age, body weight and height of subjects following baseline measures were included in the covariate screening.

Individualized baseline model development for intragastric pH

It is well known that intragastric acid secretion is circadian in nature, producing intragastric acid pH values that are higher at night and lower during the day [30] and individual gastric pH with typical food related circadian rhythm [31]. Therefore, a baseline model for this rhythm should be incorporated into the PD model to precisely estimate the drug effect.

The gastric pH of YH4808 in the 24-h circadian rhythm study was modeled by harmonic functions, as follows:

$$\text{Gastric pH} = a_0 + a_1 \cos\left[\frac{2\pi(TAD-b_1)}{24}\right] + a_2 \sin\left[\frac{2\pi(TAD-b_2)}{18}\right] + a_3 \cos\left[\frac{2\pi(TAD-b_3)}{12}\right] + a_4 \sin\left[\frac{2\pi(TAD-b_4)}{6}\right] \quad (3)$$

,where a_0 is the mean gastric pH, a_i is an amplitude, b_i is a peak time, TAD represents the time elapsed after placebo administration, and $2\pi/24$, $2\pi/18$, $2\pi/12$ and $2\pi/6$ convert time to radians.

Pharmacokinetic/pharmacodynamic model development

An effect compartment model, which assumes the rate of drug distribution to and from the hypothetical effect site will determine the rate of onset of effect, was implemented to relate plasma concentrations of YH4808 to the change of intragastric pH because the increase of intragastric pH in each subject lagged behind the plasma concentration time course of YH4808. In such a model, the time course of the effect site concentration (C_e) is described by the rate constant (k_{e0}) from the effect compartment.

A sigmoid maximum effect (E_{max}) model with a baseline effect was tried to fit the intragastric pH data, and it was simultaneously applied to predict the plasma concentration of YH4808 following single and multiple oral administration.

$$\text{Gastric pH} = E_0 \times (1 + \frac{E_{max} \times C_E}{EC_{50} + C_E}) \quad (4)$$

,where E_0 is the placebo effect (baseline), E_{max} is the maximum effect of intragastric pH, EC_{50} is the drug concentration that produces 50% of the maximal effect, and C_E is the corresponding effect compartment concentration. The IIV of the PD parameters was evaluated using an exponential error model, and the additive error model was used to present the RV of the drug effect.

Model evaluation

A visual predictive check (VPC) was performed for the evaluation of the final population PK and PK/PD models. Using the final model, 1000 simulated replicates of the original dataset were generated, and the median and the 5^{th} and 95^{th} percentiles calculated from simulated concentrations were compared with the measured concentrations. Additionally, to validate the reliability and stability of the model, a non-parametric

bootstrap analysis was performed. The final PK and PD parameters were compared with 95% confidence intervals (CIs) calculated using the 2.5 and 97.5 percentiles obtained from 1000 bootstrap estimations.

RESULTS

1. Physiologically-based pharmacokinetic (PBPK) modeling of YH4808

1.1. Caco-2 transcellular permeability

The average apparent permeability (P_{app}) for YH4808 (i.e., apical to basolateral direction) was 1.49 x 10^{-5} cm/sec over the drug concentration range of 0.1-10 μM. There was no evidence of flux saturation with increased drug concentration. YH4808 is highly permeable, i.e., P_{app} >5.0 x 10^{-6} cm/sec, indicating the compound is expected to be well absorbed through the gastrointestinal epithelial membrane [32].

1.2. Metabolic stability

The remaining percentage of parent after 30 min was 39.8 (human), 46.4 (rat), 2.6 (mouse), 21.7 (dog) and 6.1 % (monkey), and the values of the half-life ($t_{1/2}$) in human, rat, mouse, dog and monkey liver microsomes were 17.7, 28.5, 5.3, 7.5 and 3.2 min for YH4808 concentrations of 10 μM. The rapid decrease in the metabolic stability of YH4808 indicated that various metabolic pathways, mostly CYP isozymes, were

involved in the metabolism of YH4808.

1.3. Inhibition of CYP enzymes by YH4808

The IC_{50} values of CYP3A4, CYP2C9, CYP2C19, CYP2C8, CYP2A6 and CYP1A2 were 19.7, 23.9, 5.0, >25, >25 and 6.4 μM, respectively. YH4808 showed no apparent inhibition of these CYP P450 isozymes, thus, the result suggested little potential for DDIs of YH4808.

1.4. Plasma protein binding

The *in vitro* plasma protein binding rate of YH4808 was 99.17% (rats, 95% CI: 99.15−99.18%), 99.62% (dogs, 95% CI: 99.61−99.63%), 98.45% (monkeys, 95% CI: 98.40−98.47%) and 99.54% (humans, 95% CI: 99.52−99.54%), respectively.

1.5. PBPK modeling and simulation in humans: single oral administration

Physicochemical properties, combined with *in vitro* human data (clearance, permeability and plasma protein binding) and human physiological data were used to simulate human plasma concentration versus time profiles of YH4808 over a dose

range of 50−400 mg. The ratios of the human PBPK model-predicted to observed mean values of PK parameters such as C_{max} and AUC_{0-t} were not within the predefined range (0.5−2 fold). Therefore, the human PBPK model of YH4808 was further optimized using the Parameter Estimation module and plasma concentrations after a single administration in healthy volunteers at 50−400 mg. The optimized human PBPK model adequately simulated the observed plasma concentration−time profiles of YH4808 after a single oral administration over a dose range of 50 to 400 mg, particularly after optimization of intrinsic hepatic clearance and regional permeability in ADAM model (Figure 6). Furthermore, the ratios of the PBPK model-predicted to observed mean values of PK parameters such as C_{max}, T_{max} and AUC_{0-t} were all within the predefined range (0.5−2 fold) (Table 2).

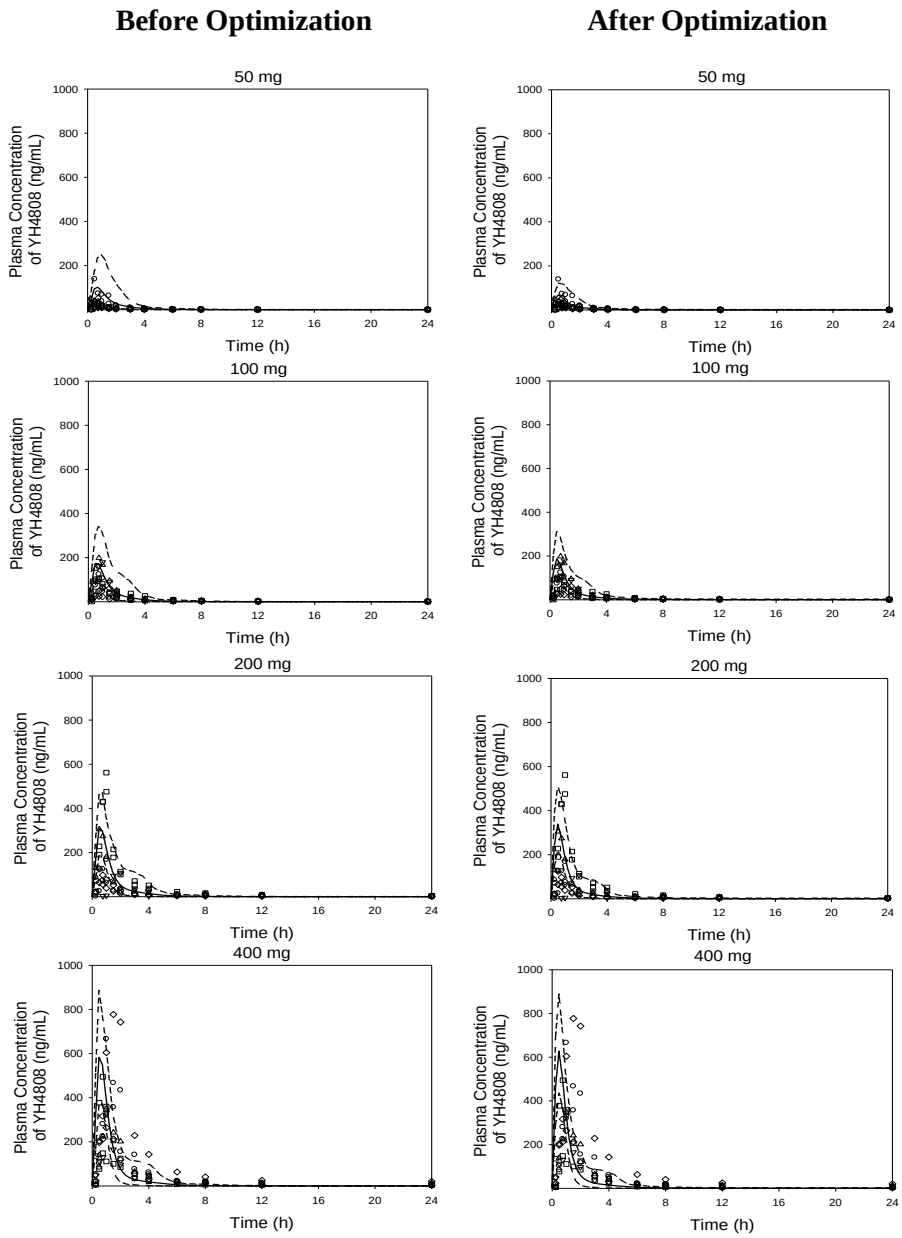

Figure 6. Observed (different symbols for different subjects) and model-predicted (—) mean plasma concentration-time profiles of YH4808 in humans after single oral administration before (a, b, c, and d) and after (e, f, g, and h) optimization. The dashed lines represent the 5^{th} and 95^{th} percentiles of model-predicted plasma concentrations.

Table 2. Comparison of the model-predicted and observed pharmacokinetic parameters for YH4808 after single oral administration in humans

Dose (mg)	Data source	Pharmacokinetic parameter					
		Before optimization			After optimization		
		C_{max} (ng/mL)	T_{max} (hr)	AUC_{0-t} (ng·hr/mL)	C_{max} (ng/mL)	T_{max} (hr)	AUC_{0-t} (ng·hr/mL)
50	Observed	47.8±40.1	0.8 (0.5-1.5)	73.4±49.1	47.8±40.1	0.8 (0.5-1.5)	73.4±49.1
	PBPK	101.9	0.7	165.3	67.9	0.5	103.3
	Fold difference	2.1	0.9	2.3	1.4	0.6	1.4
100	Observed	110.9±56.5	0.8 (0.5-1.0)	222.5±102.1	110.9±56.5	0.8 (0.5-1.0)	222.5±102.1
	PBPK	173.2	0.7	261.2	186.9	0.5	262.2
	Fold difference	1.6	0.9	1.2	1.7	0.6	1.2
200	Observed	241.8±186.2	0.8 (0.5-2.0)	427.2±274.7	241.8±186.2	0.8 (0.5-2.0)	427.2±274.7
	PBPK	308.4	0.5	419.2	338.6	0.5	420.4
	Fold difference	1.3	0.6	1.0	1.4	0.6	1.0
400	Observed	437.2±208.7	1.0 (0.7-1.5)	1077.7±645.1	437.2±208.7	1.0 (0.7-1.5)	1077.7±645.1
	PBPK	582.7	0.5	714.1	627.1	0.5	703.3
	Fold difference	1.3	0.7	0.7	1.4	0.5	0.7

C_{max}: Peak plasma concentration (ng/mL)
T_{max}: Time to reach C_{max} following drug administration (hr)
AUC_{0-t}; Area under the plasma concentration-time curve from time 0 to the time of last observable concentration (ng·hr/mL)
Fold difference: The ratio of model-predicted to observed values
Values are presented as arithmetic mean±SD, however, T_{max} values represented as median (minimum, maximum).
Each simulation was replicated 100 times.

1.6. PBPK modeling and simulation in humans: repeated oral administration

The simulated plasma concentration–time profiles of YH4808 after repeated oral administration at 100, 200 and 400 mg were in line with the observed ones (Figure 7). Likewise, the ratio of the model-predicted PK parameter to the observed value fell entirely within the pre-specified range of 0.5–2.0 (Table 3). However, the PBPK model failed to predict the decrease in the systemic exposure to YH4808 after repeated administration, particularly at 200 and 400 mg. For example, the observed C_{max} and AUC (AUC_{inf} and AUC_{τ} after a single and repeated oral administrations, respectively) of YH4808 at 400 mg were decreased by 56.3% and 46.3%, respectively, from Day 1 to Day 7 (C_{max}: 480.7 vs. 210.3 ng/mL; AUC: 1149.9 vs. 618.0 ng·hr/mL, Table 3), whereas the model-predicted C_{max} and AUC were almost the same between Days 1 and 7 (C_{max}: 589.4 vs. 592.5 ng/mL; AUC: 1322.5 vs. 1332.4 ng·hr/mL, Table 3).

A power model analysis using logarithmically transformed C_{max} and AUC_{τ} versus logarithmically transformed dose showed that the systemic exposure to YH4808 increased in a less than dose-proportional manner in the range of 100–400

mg after repeated oral administration. The slope of the regression line was 0.26 (95% CI: −0.40−0.92) and 0.75 (95% CI: 0.39−1.11) for C_{max} and AUC_{τ}, respectively, on Day 7.

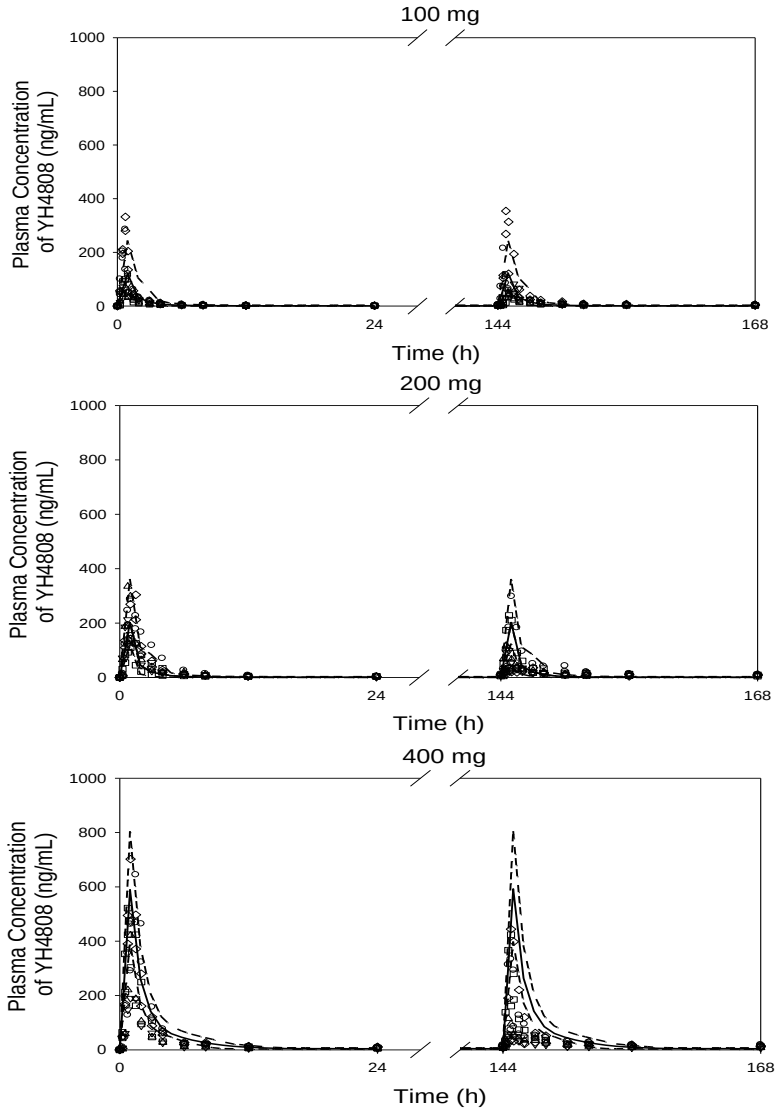

Figure 7. Observed (different symbols for different subjects) and model-predicted (—) mean plasma concentration-time profiles of YH4808 in humans after repeated oral administration at 100, 200 and 400 mg once a day. The dashed lines represent the 5^{th} and 95^{th} percentiles of model-predicted plasma concentrations. The observed plasma concentrations were obtained from subjects repeatedly administered with YH4808 at 100, 200 and 400 mg in the multiple-ascending dose portion of a phase I clinical trial with YH4808.

Table 3. Comparison of the model-predicted and observed pharmacokinetic parameters for YH4808 after repeated oral administration in humans

PK parameter	100 mg				200 mg				400 mg			
	Day 1		Day 7		Day 1		Day 7		Day 1		Day 7	
	C_{max} (ng/mL)	AUC_{inf} (ng·hr/mL)	C_{max} (ng/mL)	AUC_{τ} (ng·hr/mL)	C_{max} (ng/mL)	AUC_{inf} (ng·hr/mL)	C_{max} (ng/mL)	AUC_{τ} (ng·hr/mL)	C_{max} (ng/mL)	AUC_{inf} (ng·hr/mL)	C_{max} (ng/mL)	AUC_{τ} (ng·hr/mL)
Observed	171.5± 114.1	234.5± 99.9	142.4± 120.3	227.8± 126.0	239.1± 73.0	490.9± 140.8	115.2± 97.9	397.7± 180.4	480.7± 155.3	1149.9± 354.1	210.3± 166.8	618.0± 276.9
PBPK	120.6	220.3	121.1	225.6	201.8	362.8	202.3	364.9	589.4	1322.5	592.5	1332.4
Fold difference	0.7	0.9	0.9	1.0	0.8	0.7	1.8	0.9	1.2	1.2	2.8	2.1

C_{max}: Peak plasma concentration (ng/mL)
AUC_{inf}: Area under the plasma concentration-time curve from time 0 to infinity (ng·hr/mL)
AUC_{τ}: Area under the plasma concentration-time curve over dosing interval (ng·hr/mL)
Fold difference: The ratio of model-predicted to observed values
Values are presented as arithmetic mean±SD. Each simulation was replicated 100 times.

1.7. Model validation (DDIs)

Fluvoxamine (50 mg once daily), a strong CYP2C19 inhibitor, was predicted to increase the AUC of YH4808 only by a 1.5-fold. Likewise, fluoxetine (40 mg once daily), a strong CYP2D6 inhibitor, was predicted not to affect the AUC of YH4808 (1.0-fold increase). These simulated DDI results, i.e., no significant interactions between YH4808 and a CYP2C19 and CYP2D6 inhibitor, confirmed similar findings from the in vitro CYP inhibition study.

1.8. PBPK simulation for the effect of varying gastric pH

As the intragastric pH was increased from 1.5 to 7, the C_{max} and AUC_{0-t} of YH4808 after oral administration at 400 mg were reduced from 375.7 to 267.0 ng/mL for C_{max} and from 692.0 to 550.4 ng·hr/mL for AUC_{0-t} (Figure 8).

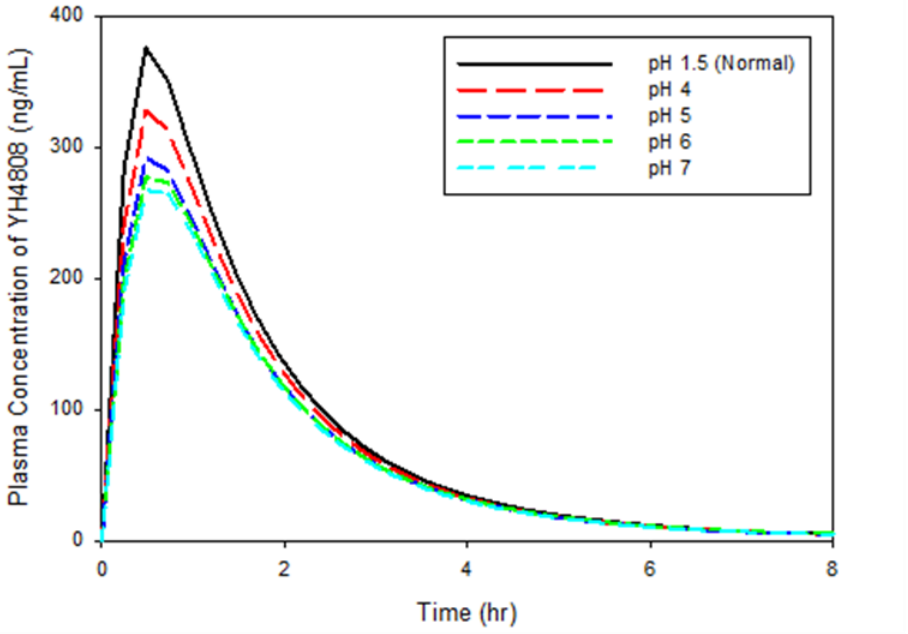

Figure 8. Model-predicted mean plasma concentration-time profiles of YH4808 after a single oral administration at 400 mg over a stomach pH range of 1.5 - 7.

2. Mechanism-based pharmacokinetic and pharmacodynamics (PK/PD) modeling of YH4808

2.1. Dataset and baseline subject demographics

A total of 123 subjects completed the clinical study (83 and 40 for the single and multiple dose studies, respectively) after having been randomly assigned to one of the dose groups in the single or multiple dose studies. The mean age and weight of the subjects were 25.5 years (range 20-41 years), and 67.5 kg (range 53.5-87.2 kg), respectively. Among the 123 subjects, 1627 plasma concentrations and 1846 intragastric pH points from 80 subjects (56 and 24 for the single and multiple dose studies, respectively) were pooled for PK/PD analysis.

2.2. Population pharmacokinetic/pharmacodynamic analysis

Pharmacokinetic model

A two-compartment model with a first-order absorption combined with lag-time adequately described the concentration-time profiles in healthy subjects following oral administration of YH4808 (Figure 9). Inter-individual

variability was estimated for the following PK parameters: apparent clearance (CL/F), apparent volumes of distribution of the central and peripheral compartments (V_C/F and V_P/F, respectively), apparent inter-compartmental clearance (Q/F), first-order absorption rate constant (Ka) and lag-time of the first-order process (ALAG1). Inter-occasion variability was not estimated for all PK parameters. Only body weight as a covariate significantly improved the model fit.

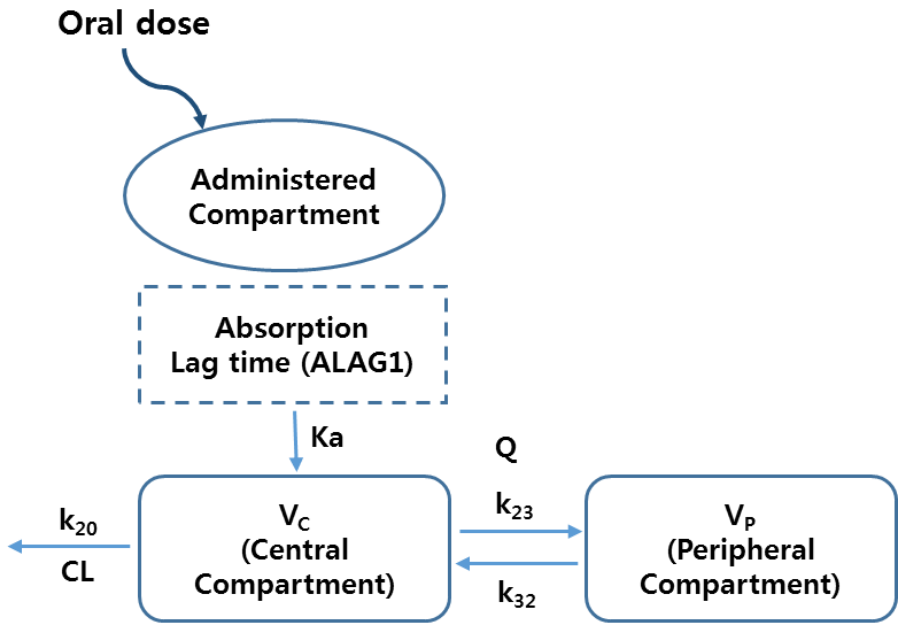

Figure 9. Schematic diagram of the final pharmacokinetic model of YH4808

The effect of covariate, body weight, on the PK parameter (CL/F) is expressed in the following equation:

$$\frac{CL}{F}\left(L/h\right) = 467 \times \left[\frac{body\ weight\ (kg)}{70}\right]^{0.94} \quad (5)$$

Therefore, in general, the body weight had a positive relationship with the clearance (CL/F) of YH4808 as expected, and the typical value of the clearance (CL/F) parameter of YH4808 would be greater in heavier subjects.

The general goodness-of-fit plots, VPC plots and the bootstrap-resampling of the final PK model showed good adequacy between the observed and the predicted YH4808 concentrations in plasma without discernible systematic bias (Figure 10 and Figure 11). The final PK model parameters were adequately estimated with median and 95% CIs generated by the bootstrap-resampled simulated trials (Table 4). In conclusion, the final PK model was robust in describing the PK characteristics of YH4808 following oral administration in healthy subjects.

Table 4. Parameters of the final pharmacokinetic model of YH4808

Parameter	Unit	Typical value [Median, 95% CI][a]	Inter-individual variability (CV%) [Median, 95% CI][a]
Apparent clearance (CL/F)	L/h	467 [467, 416-518]	58.7 [58.6, 47.2-68.2]
Body weight on CL/F[b]		0.94 [0.91, 0.6-1.2]	
Apparent volume of distribution, central compartment (V_C/F)	L	291 [234, 233-342]	91.9 [96.0, 65.0-112.5]
Apparent volume of distribution, peripheral compartment (V_P/F)	L	5230 [5233, 4501-5967]	70.5 [70.5, 50.1-86.2]
Apparent inter-compartmental clearance (Q/F)	L/h	288 [301, 233-342]	66.1 [66.1, 52.2-77.6]
First-order absorption rate constant (Ka)	h^{-1}	0.89 [0.89, 0.8-1.0]	25.5 [25.0, 12.1-37.4]
Lag-time of first-order absorption (ALAG1)	h	0.22 [0.22, 0.21-0.23]	9.1 [7.5, 1.8-12.8]
Proportional residual variability (CV%)		43.1	
Additive residual variability	ng/mL	0.01 FIX	

[a]Median value and 95% confidence intervals were derived using 1000 re-sampled bootstrap runs

[b]Power term in Equation (5)

CV%: coefficient variation expressed as percent; CI: confidence interval

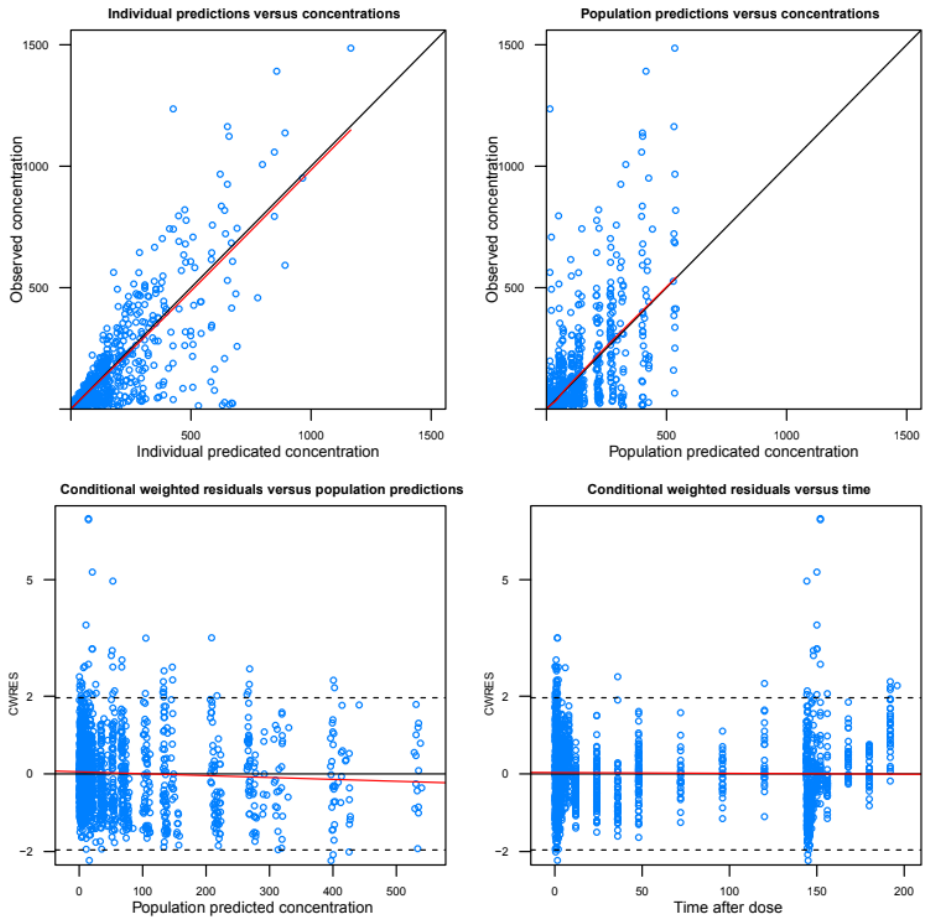

Figure 10. The basic goodness-of-fit plots of the final pharmacokinetic model of YH4808

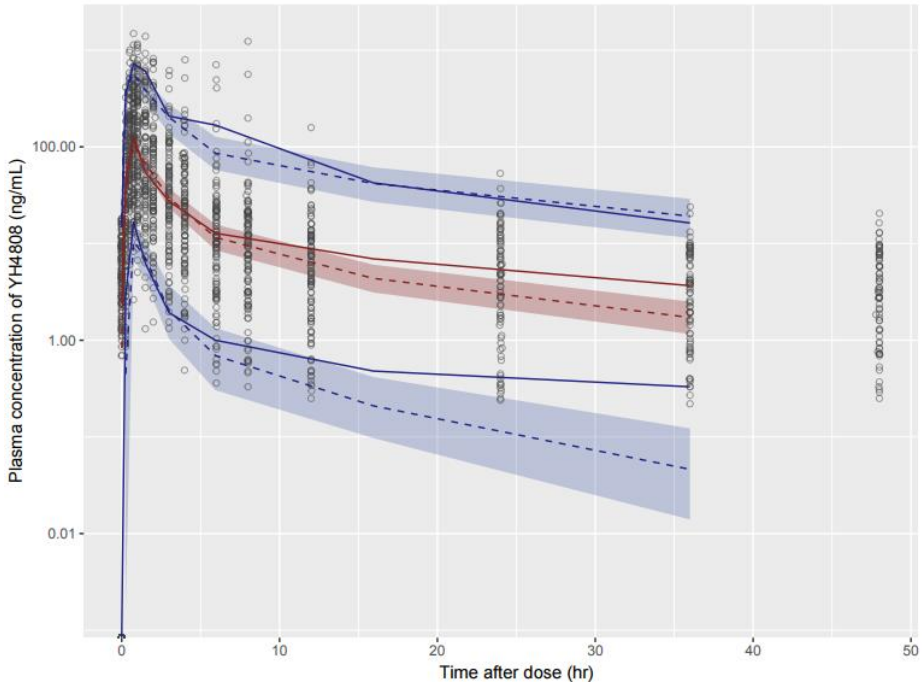

Figure 11. Visual predictive check of the final PK model of YH4808. Empty circles denote observed concentration; Solid lines represent the upper 95th, median, and lower 5th values of observed concentrations while dashed lines denote prediction, i.e., the upper 95th, median, and lower 5th values of simulated concentrations; Shaded areas denote the 95% prediction intervals around the simulated upper 95th, median, and lower 5th values, respectively, based on the final PK model. Concentrations are drawn in the logarithmic scale.

Individualized baseline model for intragastric pH

The baseline pH versus time profiles are adequately described by harmonic functions and the circadian pattern is disturbed by food intakes that can be observed as peaks in pH values (Figure

12). In addition, the rises during the later times correspond to night hours and can be explained by decreases in hydrogen secretion due to the circadian rhythm.

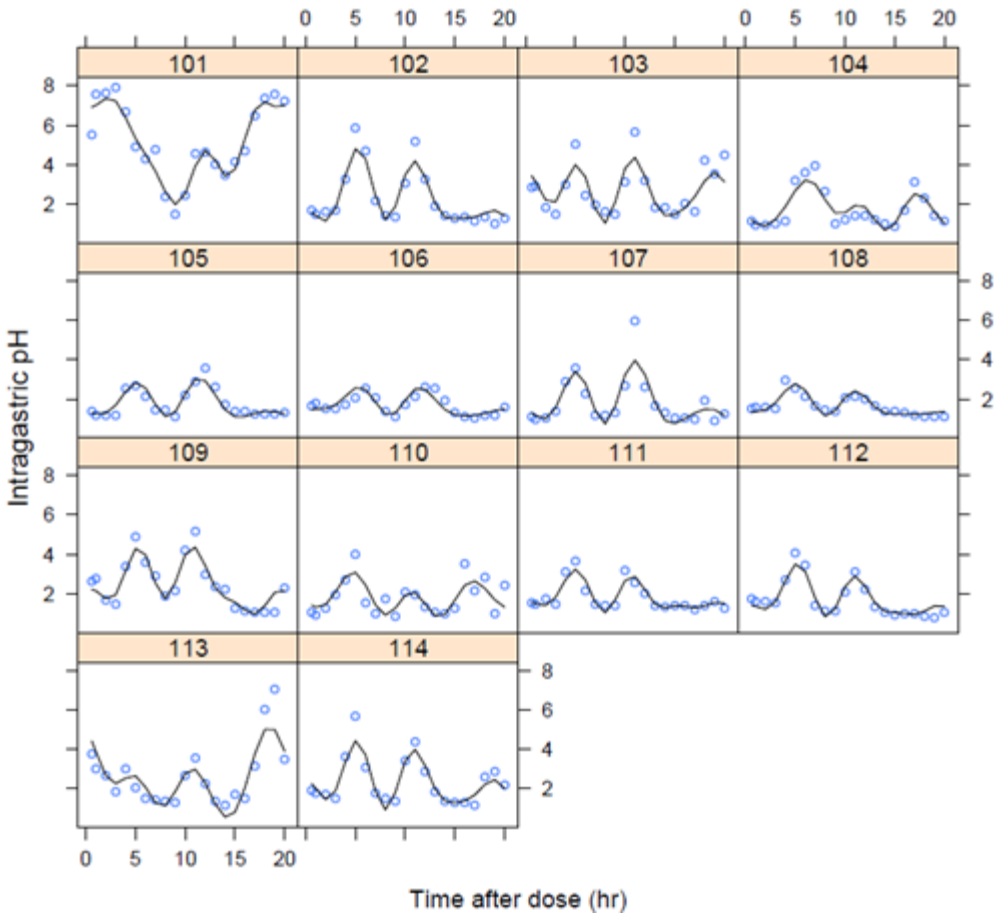

Figure 12. Individual fitting plots of intragastric pH values versus time for placebo group (101−114: subject ID number for placebo group)

Pharmacokinetic/pharmacodynamic model

The relationship between intragastric pH and plasma concentration of YH4808 is well described by the sigmoid maximum effect (E_{max}) model with an effect compartment in this study (Figure 13). In addition, to address changes in intragastric pH over time affecting the plasma concentration of YH4808, we introduced a feedback path such that increased intragastric pH decreases the relative bioavailability of YH4808, and analyzed PK and PD data simultaneously. An inhibitory effect model was used for the feedback by intragastric pH for plasma concentrations of YH4808, as follows:

$$\text{Feedback} = 1 - \frac{ED_{max} \cdot Intragastric\ pH}{ED_{50} + Intragastric\ pH} \quad (6)$$

,where ED_{max} is the maximum reduction of the relative bioavailability of YH4808 and ED_{50} is the intragastric pH that produces 50% of maximum reduction of the relative bioavailability. The IIV of these parameters was evaluated using an exponential error model, and the RV was evaluated using an additive random effect model. After evaluation of the OFV and the model fit, the final PK/PD model was selected including IIV on the E_{max}, EC_{50}, k_{e0}, ED_{max} and ED_{50}.

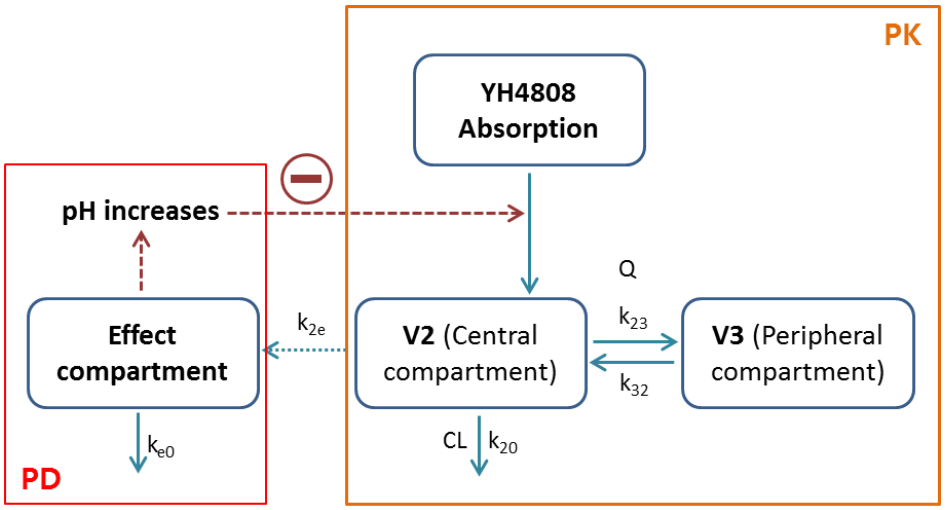

Figure 13. Schematic diagram of the final mechanism-based pharmacokinetic and pharmacodynamic model of YH4808.
A sigmoid E_{max} model with baseline effect was used for linking the changes in intragastric pH to the PK model as follows: $E_0 \times [(E_{max} \times C_e)/(EC_{50} + C_e)]$. An inhibitory E_{max} model for the feedback was introduced to address changes in intragastric pH over time affecting the plasma concentration of YH4808. The feedback interaction is shown with red dashed line.

Table 5. Parameters of the final pharmacokinetic/pharmacodynamic model of YH4808

Parameter	Unit	Typical value [95% CI]	Inter-individual variability (CV%)
E_{max}	–	1.08 [0.518-1.642]	278.3
EC_{50}	ng/mL	234.0 [124.0-344.0]	26.3
k_{e0}	h^{-1}	0.07 [0.036-0.112]	59.4
ED_{max}	–	0.405 [0.321-0.489]	49.6
ED_{50}	–	2.987 [2.221-3.753]	28.0
Additive residual variability	–	1.34	–

RSE: Relative standard error, CI: confidence interval, CV%: coefficient variation expresses as percent
E_{max}: maximum effect
EC_{50}: plasma concentration producing 50% of maximal effect
k_{e0}: rate constant for elimination from effect compartment
ED_{max}: maximal reduction of relative bioavailability
ED_{50}: intragastric pH producing 50% of maximal reduction of relative bioavailability

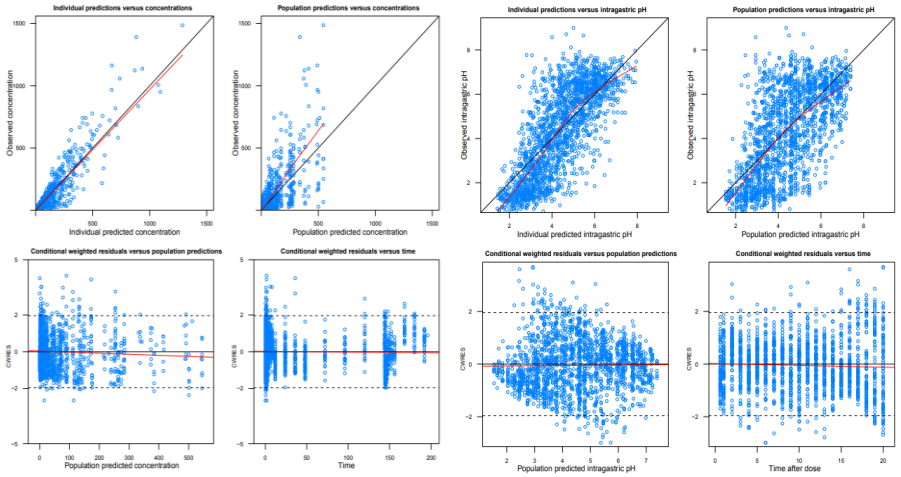

Figure 14. The basic goodness-of-fit plots of the final pharmacokinetic and pharmacodynamic model of YH4808: pharmacokinetic model (left); pharmacodynamic model (right)

DISCUSSION

In this study, the PBPK and PK/PD models developed using combined bottom-up and top-down approaches (i.e., middle-out approach) were able to capture mechanistically the inter-relationship between plasma concentrations of YH4808 and intragastric pH profiles over 24 hour period after single and multiple administrations of YH4808 in humans. The reduced solubility of YH4808 by elevated intragastric pH after oral administration was hypothesized as the main cause of the decrease in exposure, and this hypothesis was confirmed by PBPK modeling and simulation. In addition, the PK/PD model adequately described quantitative mutual relationships between the exposure to YH4808 and intragastric pH by introducing a feedback loop such that increased intragastric pH decreases the relative bioavailability of YH4808. As a whole, the potential mechanism of YH4808 that the decrease of the relative bioavailability was caused by elevated intragastric pH was confirmed by the PBPK model, and this mechanism based PK/PD model best described the decrease in the systemic exposure of YH4808 after multiple oral administration.

In PBPK modeling study, the human PK parameters of

YH4808 estimated by optimized PBPK model using the ADAM module were similar to the observed ones after a single oral administration at 50−400 mg (Table 2 and Figure 6). However, the human PBPK model failed to predict the decrease in the systemic exposure to YH4808 after repeated oral administration, particularly at higher doses such as 200 and 400 mg (Figure 7) although the ratio of the model−predicted PK parameter to the observed value fell entirely within the pre−specified range of 0.5−2.0 (Table 3).

Several hypotheses can be proposed. First, the low oral bioavailability of YH4808 along with its huge interindividual variability (mean: 10.1%, range: 2.3−19.3%) might have contributed to the reduced exposure to YH4808 after multiple administration [14]. This mechanism, however, does not appear to fully explain the decrease in the systemic exposure to YH4808 after repeated oral administration because the decreased exposure was seen rather consistently at all doses studied. Second, altered drug metabolism and transporter activities for YH4808, particularly after repeated administration, could be another possibility. However, YH4808 did not induce the CYP450 isozymes in human hepatic microsomes. Furthermore, YH4808 has a high permeability (1.49×10^{-5}

cm/sec) and is not a substrate of efflux transporters based on the Caco-2 cell permeability study, suggesting altered drug metabolism and transporter activities was less likely [32,33].

Therefore, we should consider other explanations, which are mechanistically more plausible. Changes in biopharmaceutical properties such as solubility after repeated oral administration with YH4808 can be a candidate. YH4808 has a pH-dependent solubility; the solubility of YH4808 is dramatically decreased as pH is increased, e.g., 2.137 and 0.046 mg/mL at pH 2.0 and 6.0, respectively (Table 1). Repeated oral administration of YH4808 is expected to increase intragastric pH similar to that in the small and large intestines because acid secretion in the stomach is inhibited. To support this notion, the intragastric pH remained high (i.e., pH >4) over 24 hours after repeated oral administration of YH4808 at 400 mg once daily [10]. Consequently, an approximately 50-fold decrease in solubility of YH4808 after multiple administration could have negatively affected the absorption of YH4808.

Based on the hypothesis, we investigated the effect of increased intragastric pH on the exposure to YH4808 using the SimCYP® Simulator. As we varied intragastric pH from 1.5 (i.e., normal physiology in the fasting state) to 4 to 7, the PK profiles

of orally-administered YH4808 was simulated. In this simulation, no assumption was made as to precipitation time because slow dissolution of YH4808 in the elevated gastric pH is not expected to cause supersaturation in the small intestine [24]. As intragastric pH was increased from 1.5 to 7, the C_{max} and AUC_{0-t} of YH4808 after oral administration at 400 mg were reduced by 12.7-28.9% and 7.9-18.6%, respectively (Figure 8). Therefore, the decrease in the exposure to YH4808 after repeated administration (Figure 7(b)-(c)) could have been most likely caused by the reduced solubility of YH4808 as the intragastric pH was increased. Similarly, elevated gastric pH induced by concomitantly-administered ARAs decreased the exposure of weak base drugs having pH-dependent solubility.[14] For example, palbociclib, a highly selective inhibitor of cyclin-dependent kinase 4 and 6, showed a reduced C_{max} and AUC_{0-t} by 80% and 62%, respectively, when co-administered with rabeprazole, an ARA [34].

This study had some limitations. First, our simulation based on increased intragastric pH, which was chosen rather arbitrarily, did not reflect its dynamic changes over time. Therefore, the effect of increased intragastric pH on the exposure to YH4808 was static at best. Second, the observed

decrease in the exposure to YH4808 after repeated administration was larger than those simulated with intragastric pH being increased from 1 to 7 (56.3% vs. 28.9% for C_{max}; 46.3% vs. 20.5% for AUC_{0-t}). Therefore, there might be other factors than the decreased solubility that could explain the additional decrease in the exposure to YH4808 after repeated administration. Third, the effect of increased intragastric pH was not incorporated in the final human PBPK model. Therefore, we could not evaluate if the model's predictive performance was improved when the pH-dependent solubility of YH4808, particularly after repeated administration, was adequately integrated into the model. A more appropriate PBPK model should include the effect of change in intragastric pH by YH4808 on its PK. However, this model requires a deeper, quantitatively more complex understanding on the PK/PD relationship between YH4808 and intragastric pH. Thus, we have carried out the PK/PD analysis in the next part of our study. Even with all these limitations, however, we believe that the pH-dependent solubility of YH4808 was still the main mechanism for the reduced exposure after repeated oral administration as we showed in a prediction of varying intragastric pH (Figure 8).

To solve the last limitation of the PBPK modeling and simulation as mentioned above, we developed the mechanism-based PK/PD model of YH4808 using clinical data of phase I study. The mechanism such that increased intragastric pH decreases the relative bioavailability was confirmed in our PBPK modeling and simulation study of YH4808. This mechanism was applied to the PK/PD model to mechanistically explain the relationship of PK and PD of YH4808. A mechanism-based PK/PD model generally contains specific expressions for the characterization of processes on the causal path between drug exposure and response [35]. In our PK/PD model, we assessed inter-relationships between the time course of intragastric pH and that of the plasma concentration of YH4808. Intragastric pH profiles in a placebo group would be helpful to estimate the food effect and circadian rhythm robustly because there would be no drug effect in this group. The circadian rhythm pattern of intragastric pH is a consequence of the circadian rhythm of hydrogen secretion. The mechanism of alteration of hydrogen secretion by the inactivation of the H^+/K^+-ATPase enzyme has been modeled previously [36]. The baseline effect of intragastric pH in the PK/PD model also accounts for the circadian rhythm of

hydrogen ion production and the effects of food intake. Plotting of individual plasma concentrations of YH4808 with concurrent intragastric pH values showed a counterclockwise hysteresis loop for each subject. This hysteresis was caused by a delayed occurrence of the maximum response relative to the time course of YH4808 concentration. The observed delay between concentration and response in this study is consistent with earlier studies on PK/PD relationships of ARAs [37,38]. The hypothetical effect compartment was integrated our PK/PD model because it has been commonly applied when anticlockwise hysteresis is present in the concentration–effect plot.

In addition, a feedback path was introduced to explain the effect of increased intragastric pH on the systemic exposure of YH4808 in healthy subjects. In previous studies, an interaction between drug responses (i.e., drug effect) and PK characteristics of drug was explained using a feedback mechanism. For example, the population PK/PD model of pegfilgrastim, a PEGylated form of the recombinant human granulocyte colony–stimulating factor analog filgrastim to stimulate bone marrow to produce more neutrophils, included a bidirectional PK/PD system of pegfilgrastim, where

pegfilgrastim stimulated the proliferation, maturation, and margination of neutrophils and where circulating neutrophils in turn increased the elimination of pegfilgrastim [39]. Due to the bidirectional nature of the system where PK influences PD and PD influences the elimination of pegfilgrastim, the population PK/PD model of pegfilgrastim introduced a feedback path. Another example of feedback mechanism in PK/PD analysis was recombinant human erythropoietin (rHuEPO) [40]. The mechanism-based PK/PD model of rHuEPO was developed to describe the relationship between rHuEPO concentrations and the hematological responses to rHuEPO over time, which, in turn, drive a time-dependent change in rHuEPO elimination. In other words, the negative feedback from red blood cells accounted for the time-dependent rHuEPO clearance decline. As in the examples above, a feedback mechanism that PD influences PK was only used a PK/PD analysis of biologics in previous studies.

Our study was the first attempt to introduce a feedback path such that increased intragastric pH (i.e., PD) decreases the relative bioavailability (i.e., PK) of YH4808, a small molecule drug. Mechanistically, the superiority of the feedback model conforms to the assumed action of intragastric pH on the

relative bioavailability of YH4808. The result of the proposed feedback path was well captured the decreased exposure at Day 7 after multiple administration of YH4808.

CONCLUSION

In conclusion, first, a human PBPK model adequately predicted the concentrations of YH4808 observed in a clinical study after single and repeated oral administrations. Furthermore, a simulation experiment based on the human PBPK model indicated that the pH-dependent solubility of YH4808 could have resulted in the reduced exposure after multiple administration. PBPK modeling and simulation is a useful tool to investigate the impact of the biopharmaceutical properties of a compound on its PK profiles during clinical development. Second, a mechanism-based PK/PD model adequately described quantitative relationships between the plasma concentrations of YH4808 and the time course of intragastric pH after single and multiple oral administrations in humans. Our approach using a feedback mechanism in the PK/PD analysis is the first mechanistic modeling of a small molecule drug to describe the dynamics of the changes in intragastric pH following an ARA with pH-dependent solubility. Our analysis provides mechanistic insight into the relationship between the exposure to YH4808 and intragastric pH, which will allow for devising optimal dosing regimens for YH4808 in

future clinical studies.

REFERENCES

1. Gedda, K., Briving C., Svensson, K., Maxvall, I., and Andersson, K., *Mechanism of action of AZD0865, a K+-competitive inhibitor of gastric H+,K+-ATPase.* Biochem Pharmacol, 2007. **73**(2): p. 198-205.
2. Nilius, B., *Reviews of Physiology, Biochemistry and Pharmacology* (Springer-Verlag, 2006).
3. Maradey-Romero, C., and Fass, R., *New and Future Drug Development for Gastroesophageal Reflux Disease.* J Neurogastroenterol Motil, 2014. **20**(1): p. 6-16.
4. Andersson, K., and Carlsson, E., *Potassium-competitive acid blockade: A new therapeutic strategy in acid-related diseases.* Pharmacol Therapeut, 2005. **108**(3): p. 294-307.
5. Wurst, W., and Hartmann, M.,*Current status of acid pump antagonists (reversible PPIs).* Yale J Biol Med, 1996. **69**(3): p. 233-43.
6. Yu, K.S., et al., 2004. Pharmacokinetic and pharmacodynamic evaluation of a novel proton pump inhibitor, YH1885, in healthy volunteers. J Clin Pharmacol, 2004. **44**(1): p. 73-82.

7. Mejia, A., and Kraft, W.K., *Acid peptic disease: pharmacological approach to treatment.* Expert Rev Clin Pharmacol, 2009. **2**: p. 295-314.

8. Shin, J.M., and Sachs, G., *Pharmacology of proton pump inhibitors.* Curr Gastroenterol Rep, 2008. **10**: p. 528-34.

9. Vakil, N., *New pharmacological agents for the treatment of gastro-oesophageal reflux disease.* Aliment Pharmacol Ther, 2004. **19**(10): p. 1041-49

10. Yi, S., et al., *A novel K+ competitive acid blocker, YH4808, sustains inhibition of gastric acid secretion with a faster onset than esomeprazole: randomised clinical study in healthy volunteers.* Aliment Pharmacol Ther, 2017. **46**(3): p. 337-46.

11. Oh, S.W., et al., *YH4808, a Potent, Highly Selective K+-Competitive Acid Blocker, Suppressed Rat Acute Reflux Esophagitis More Effectively Than Esomeprazole.* Gastroenterology, 2013. **144**(5): Supplement 1, S-857.

12. Edginton, A.N., Theil, F-P., Schmitt, W., and Willmann, S., *Whole body physiologically-based pharmacokinetic models: their use in clinical drug development.* Expert Opin Drug Metab Toxicol, 2008. **4**(9): p. 1143-52.

13. Maharaj, A.R., and Edginton, A.N., *Physiologically Based Pharmacokinetic Modeling and Simulation in Pediatric Drug Development.* CPT: Pharmacometrics Syst Pharmacol, 2014. **3**(11): p. e148.

14. Jones, H.M., et al., *Physiologically based pharmacokinetic modeling in drug discovery and development: A pharmaceutical industry perspective.* Clin Pharmacol Ther, 2015. **97**(3): p. 247-62.

15. Zhuang, X., and Lu, C., *PBPK modeling and simulation in drug research and development.* Acta Pharma Sin B, 2016. **6**(5): p. 430-40.

16. Parrott, N.J., et al., *Physiologically based absorption modeling to explore the impact of food and gastric pH changes on the pharmacokinetics of alectinib.* AAPS J, 2016. **18**: p. 1464-74.

17. Parrott, N., Lukacova, V., Fraczkiewicz, G., and Bolger, M.B., *Predicting parmacokinetics of drugs using physiologically based modeling - application to food effects.* AAPS J, 2009. **11**: p. 45-53.

18. Mould, D.R., and Upton, R.N., *Basic concepts in population modeling, simulation, and model-based drug*

development. CPT: Pharmacometrics Syst Pharmacol, 2012. **1**: p. e6.

19. Mould, D.R., and Upton, R.N., *Basic concepts in population modeling, simulation, and model-based drug development—part 2: introduction to pharmacokinetic modeling methods.* CPT: Pharmacometrics Syst Pharmacol, 2013. **2**: p. e38.

20. Derendorf, H., and Meibohm, B., *Modeling of pharmacokinetic/pharmacodynamic (PK/PD) relationships: Concepts and Perspectives.* Pharmaceutical Research, 1999. **16**(2): p. 176-185.

21. Blesch, K.S., et al., *Clinical pharmacokinetic/pharmacodynamic and physiologically based pharmacokinetic modeling in new drug development: The capecitabine experience.* Investigational New Drugs, 2003. **21**: p. 195-223.

22. Perloff, E.S., et al., *Validation of cytochrome P450 time-dependent inhibition assays: a two-time point IC_{50} shift approach facilitates k_{inact} assay design.* Xenobiotica, 2009. **39**(2): p. 99-112.

23. Krippendorff, B-F., Lienau, P., Reichel, A., and Huisinga, W., *Optimizing Classification of Drug-Drug Interaction*

Potential for CYP450 Isoenzyme Inhibition Assays in Early Drug Discovery. J Biomol Screemn, 2007. **12**(1): p. 92-9.

24. The nonclinical study of YH4808 for a new drug of GERD and PUD, Health & Medical Technology R&D program. Korea Health Industry Development Institute, 2010.

25. Rodgers T., Leahy D., and Rowland M., *Physiologically based pharmacokinetic modeling 1: predicting the tissue distribution of moderate-to-strong bases.* J Pharm Sci, 2005. **94**(6): p. 1259-76.

26. Rodgers T., and Rowland M., P*hysiologically based pharmacokinetic modeling 2: predicting the tissue distribution of acids, very weak bases, neutrals and zwitterions.* J Pharm Sci, 2006. **95**(6): p. 1238-57.

27. Clinical Drug Interaction Studies – Study Design, Data Analysis, and Clinical Implications Guidance for Industry. Center for Drug Evaluation and Research. FDA, 2017.

28. Jones, H.M., Parrott, N., Jorga, K., and Lavé, T., *A Novel Strategy for Physiologically Based Predictions of Human Pharmacokinetics.* Clin Pharmacokinet, 2006. **45**(5): p. 511-42.

29. Li, G.F., et al., *Simulation of the pharmacokinetics of bisoprolol in healthy adults and patients with impaired renal function using whole-body physiologically based pharmacokinetic modeling.* Acta Pharmacol Sin, 2012. **33**(11): p. 1359-71.

30. Moore, J.G., and F. Halberg., *Circadian rhythm of gastric acid secretion in men with active duodenal ulcer.* Dig Dis Sci, 1986. **31**(11): p. 1185-91.

31. Duroux, P., et al., *Early dinner reduces nocturnal gastric acidity.* Gut, 1989. **30**(8): p. 1063-7.

32. Artursson, P., and Karlsson, J., *Correlation between oral drug absorption in humans and apparent drug permeability coefficients in human intestinal epithelial (Caco-2) cells.* Biochem Biophys Res Commun, 1991. **175**(3): p. 880-5.

33. Huang, L., et al., *Relationship between passive permeability, efflux, and predictability of clearance from in vitro metabolic intrinsic clearance.* Drug Metab Dispos, 2010. **38**(2): p. 223-31.

34. Wu, F., et al., *Predicting nonlinear pharmacokinetics of omeprazole enantiomers and racemic drug using physiologically based pharmacokinetic modeling and*

simulation: application to predict drug/genetic interactions. Pharm Res, 2014. **31**(8): p. 1919-29.

35. Danhof, M., et al., *Mechanism-based pharmacokinetic-pharmacodynamic (PK-PD) modeling in translational drug research.* Trends Pharmacol Sci, 2008. **29**(4): p. 186-91.

36. Katahima, M., et al., *Comparative pharmacokinetic/pharmacodynamic analysis of proton pump inhibitors omperazole, lansoprazole and pantoprazole in humans.* Eur J Drug Metab Pharmacokinet, 1998. **23**: p. 19-26.

37. Sanders, S.W., Buchi, K.N., Moore, J.G., and Bishop, A.I., *Pharmacodynamics of intravenous ranitidine after bolus and continuous infusion in patients with healed duodunal ulcers.* Clin Pharmacol Ther, 1989. **46**: p. 545-51.

38. Blumer, J.L., et al., *Pharmacokinetic determination of ranitidine pharmacodynamics in pediatric ulcer disease.* J Pediatr, 1985. **107**: p. 301-306.

39. Brekkan, A., et al., *A population pharmacokinetic-pharmacodynamic model of pegfilgrastim.* The AAPS journal, 2018. **20**: p. 91.

40. Ait-Oudhia, S., Schermann, J-M., and Krzyzanski, W., *Simultaneous pharmacokinetics/pharmacodynamics modeling of recombinant human erythropoietin upon multiple intravenous dosing in rats.* J Pharmacol Exp Ther, 2010. **334**(3): p. 897-910.

APPENDIX

1. Individual fitting plots for the final pharmacokinetic model of YH4808 (DV: dependent variable, IPRED: individual predicted values)

Single ascending dose groups: ID 1101−1111: 30 mg; ID 1201−1211: 50 mg; ID 1301−1312: 100 mg; ID 1401−1409: 200 mg; ID 1502−1513: 400 mg; ID 1604−1610: 600 mg; ID 1701−1713: 800 mg

Multiple ascending dose groups: ID 2301−2311: 100 mg; ID 2402−2418: 200 mg; ID 2505−2513: 400 mg

OCC=1: Day 1; OCC=3: Day 7 of multiple ascending dose study.

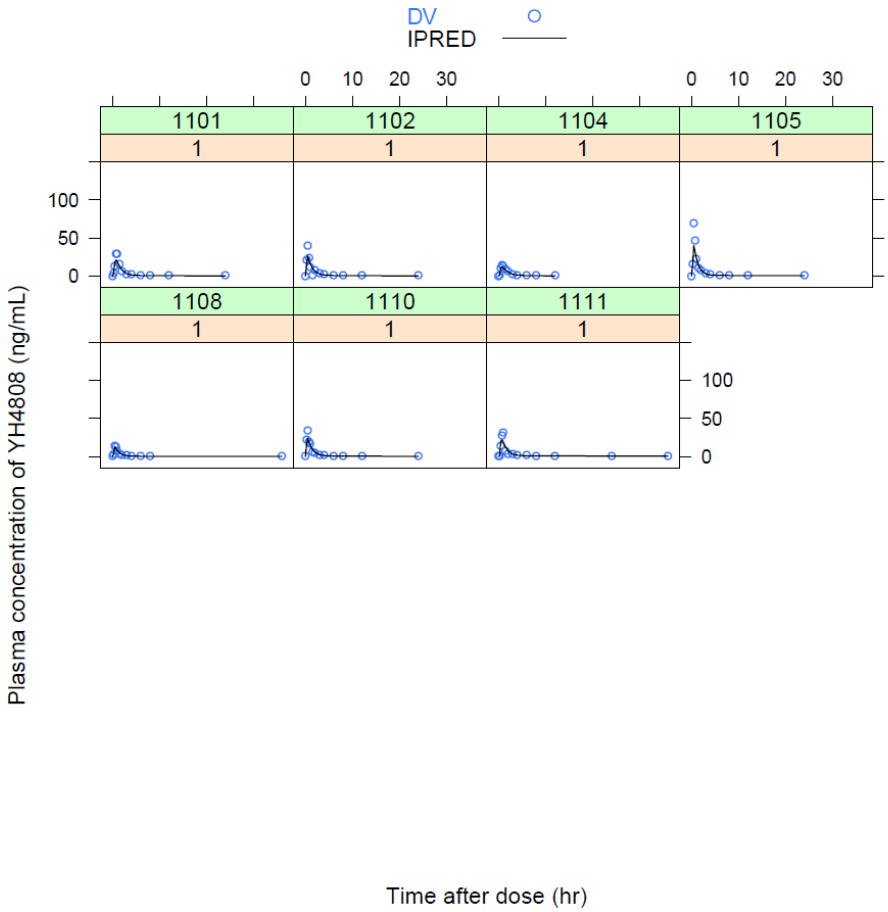

Individual fitting plots for the final pharmacokinetic model of YH4808 (DV: dependent variable, IPRED: individual predicted values) (continued)

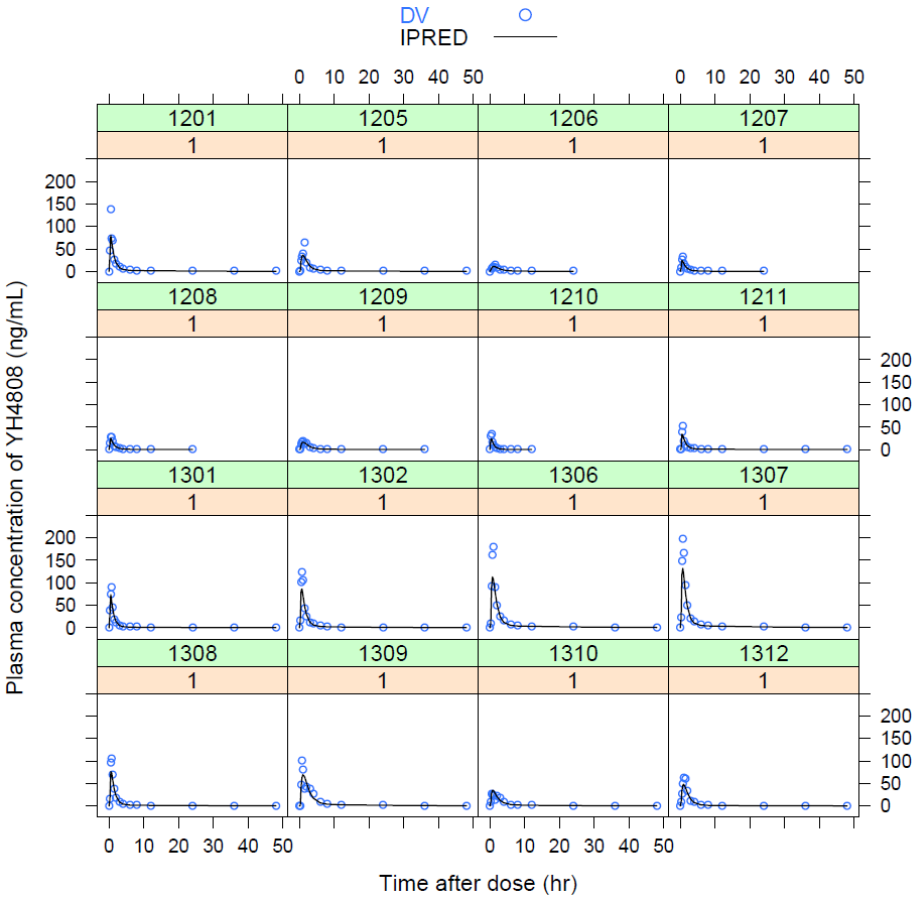

Individual fitting plots for the final pharmacokinetic model of YH4808 (DV: dependent variable, IPRED: individual predicted values) (continued)

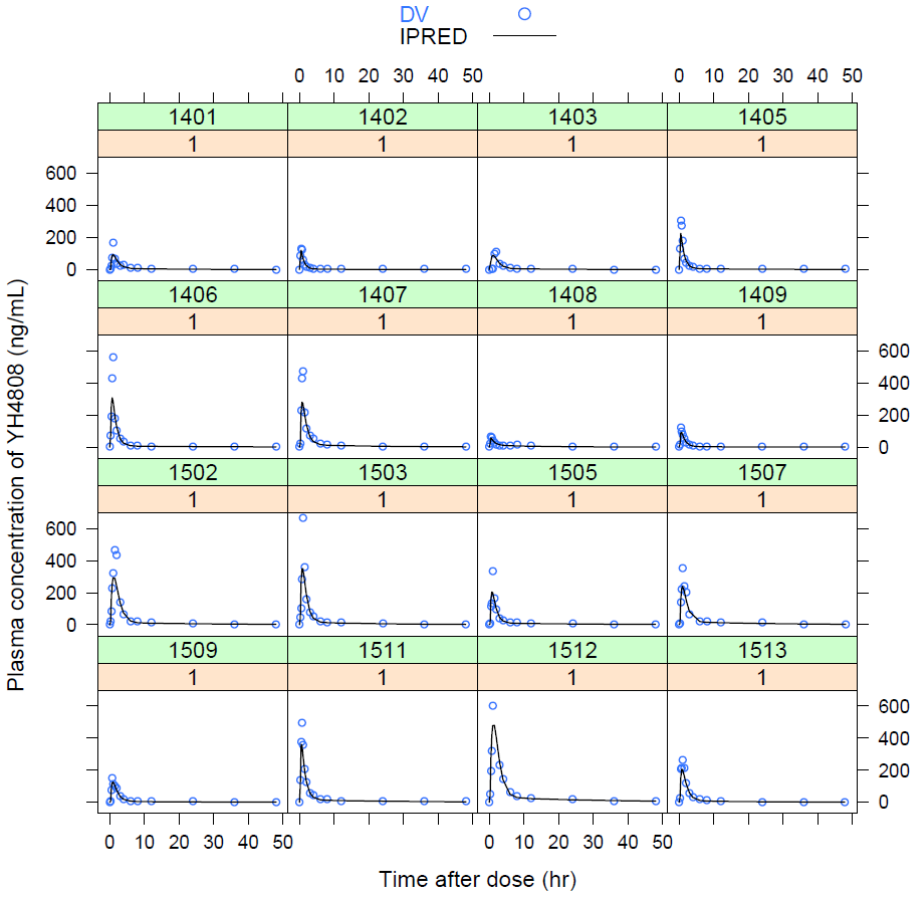

Individual fitting plots for the final pharmacokinetic model of YH4808 (DV: dependent variable, IPRED: individual predicted values) (continued)

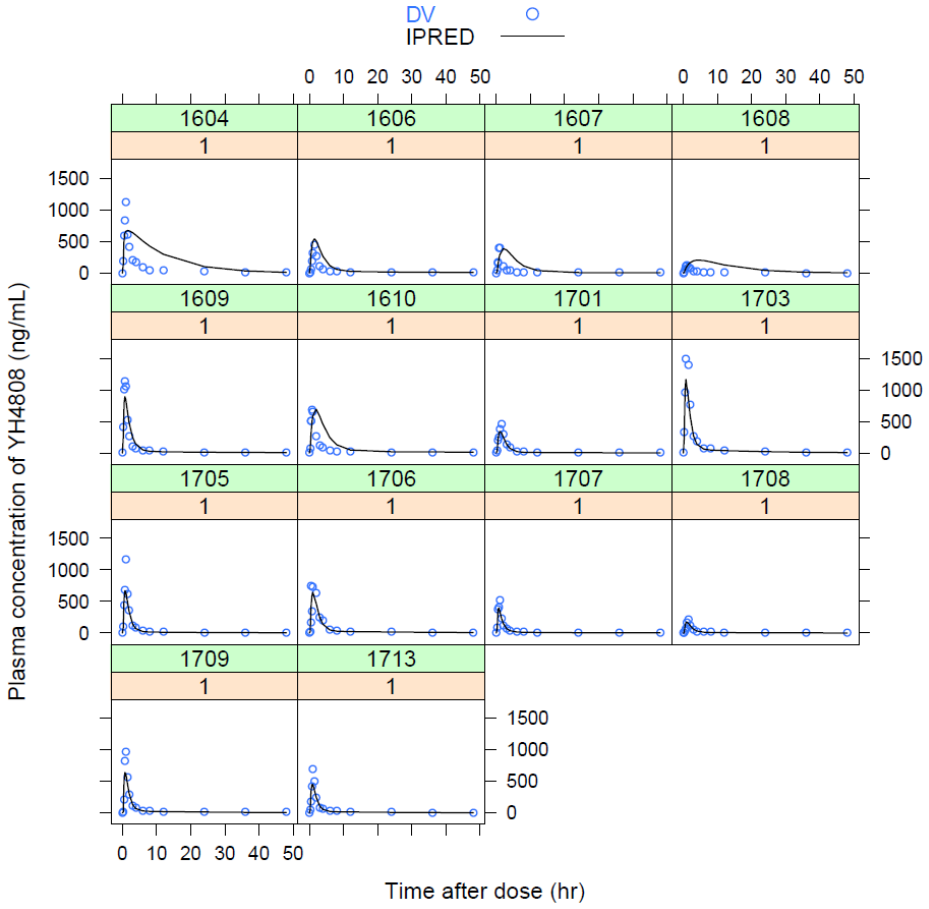

Individual fitting plots for the final pharmacokinetic model of YH4808 (DV: dependent variable, IPRED: individual predicted values) (continued)

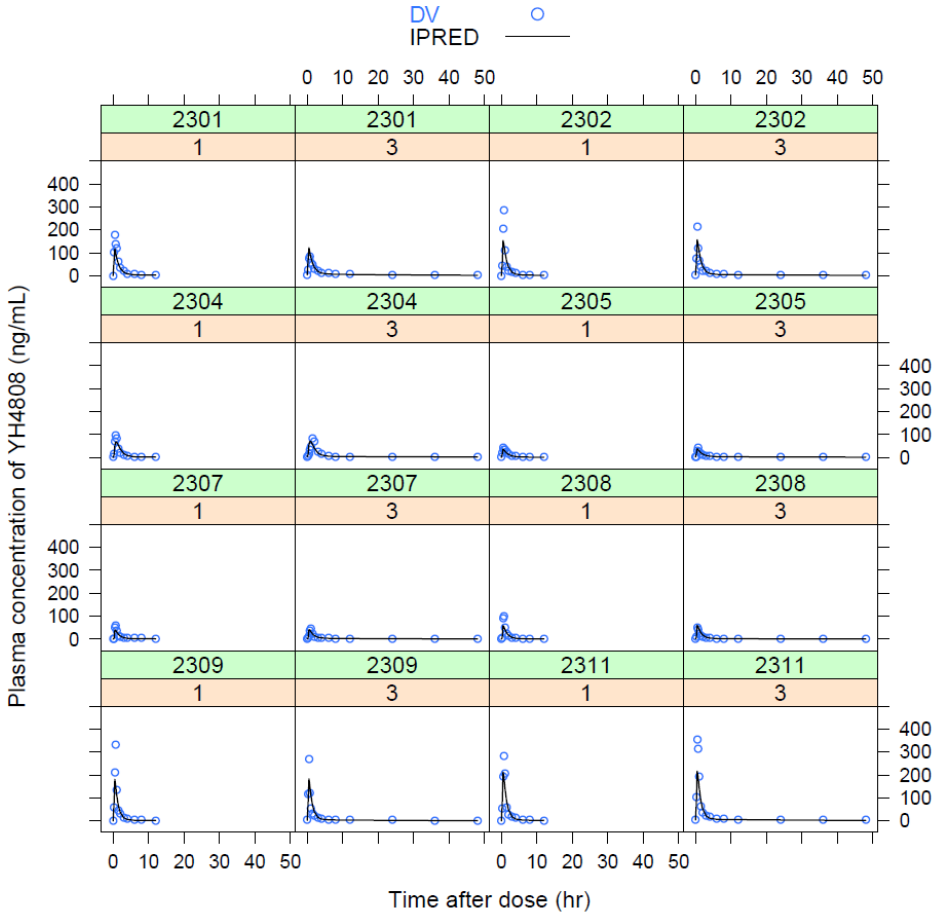

Individual fitting plots for the final pharmacokinetic model of YH4808 (DV: dependent variable, IPRED: individual predicted values) (continued)

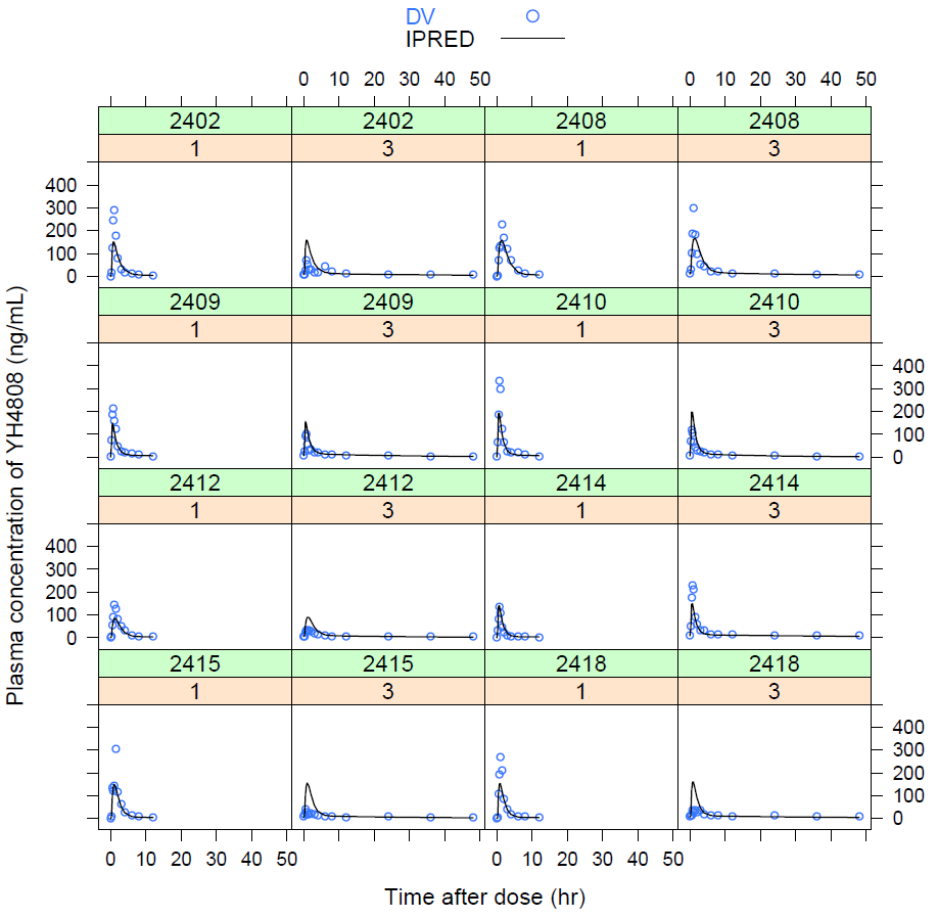

Individual fitting plots for the final pharmacokinetic model of YH4808 (DV: dependent variable, IPRED: individual predicted values) (continued)

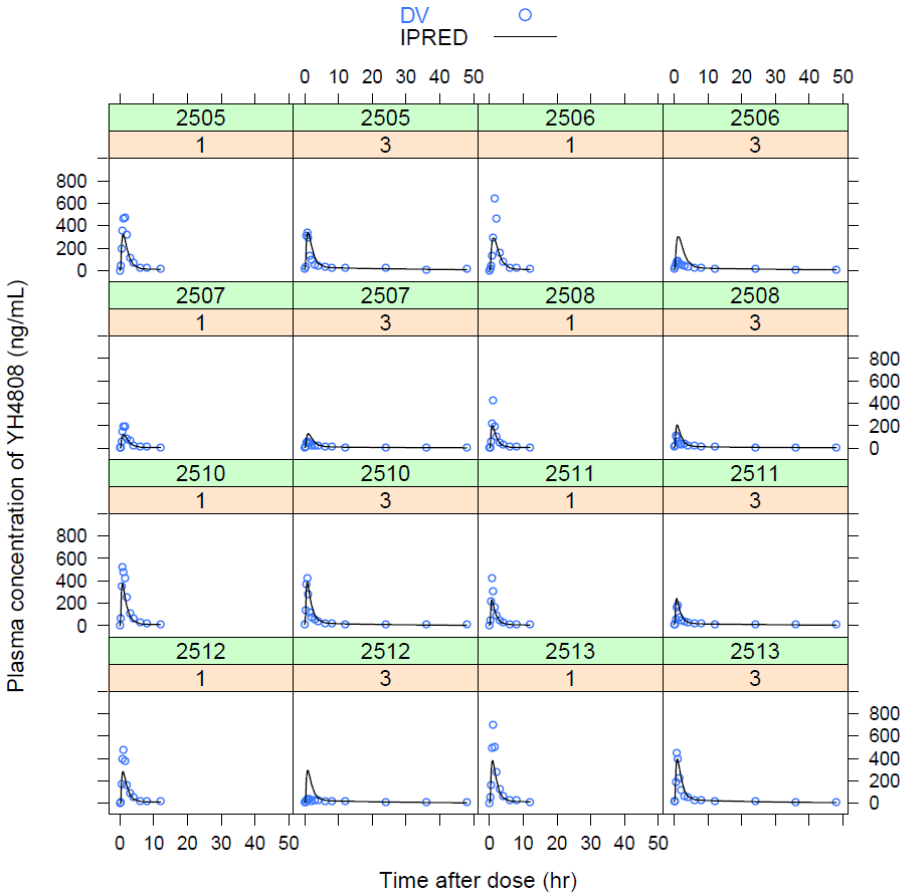

2. NONMEM control stream of the final PK model

```
$SUBROUTINE ADVAN13 TOL=4

$MODEL  COMP=(GUT) COMP=(CENTRAL) COMP=(PERIPH)

$PK

CL = THETA(1)*EXP(ETA(1))*(WT/70)**THETA(9);

V2 = THETA(2)*EXP(ETA(2))

Q = THETA(3)*EXP(ETA(3))

V3 = THETA(4)*EXP(ETA(4))

KA = THETA(5)*EXP(ETA(5))

ALAG1 = THETA(6)*EXP(ETA(6))

S2 = V2

K20 = CL/V2

K23 = Q/V2

K32 = Q/V3

K12 =KA

$DES

CP = A(2)/V2

DADT(1) = -KA*A(1)

DADT(2) = -K23*A(2)-K20*A(2)+K32*A(3)+KA*A(1)

DADT(3) = -K32*A(3)+K23*A(2)

$ERROR

IPRED = F

    W = SQRT(THETA(7)**2*IPRED**2 + THETA(8)**2)

    Y = IPRED + W*EPS(1)

 IRES = DV-IPRED

IWRES = IRES/W



$THETA

 (0,500) ; CL

 (0,500) ; V2

 (0,500) ; Q

 (0,5000) ; V3
```

```
 (0,1) ; KA

 (0,0.1) ; ALAG1

 (0,.5) ; Prop.RE (sd)

 0.01 FIX ; Add.RE (sd)

 (0,1) ; power term for BW


$OMEGA

 0.3  ;      IIV CL

 0.3  ;      IIV V2

 0.3  ;      IIV Q

 0.3  ;      IIV V3

 0.3  ;      IIV KA

 0.3  ;      IIV ALAG1


$SIGMA  1  FIX  ; Proportional error PK

$ESTIMATION METHOD=1 INTER MAXEVAL=9999 NOABORT
SIGL=3 NSIG=1 PRINT=5 POSTHOC

$COVARIANCE

$TABLE      ID TIME TAD OCC DV MDV EVID IPRED IWRES
CWRES ONEHEADER NOPRINT FILE=sdtab150

$TABLE      CL V2 V3 KA Q K20 K23 K32 ALAG1 FIRSTONLY
ONEHEADER NOPRINT NOAPPEND FILE=patab150
```

3. Individual fitting plots for the final pharmacokinetic and pharmacodynamic model of YH4808 (DV: dependent variable, IPRED: individual predicted values)

Single ascending dose groups: ID 1101−1111: 30 mg; ID 1201−1211: 50 mg; ID 1301−1312: 100 mg; ID 1401−1409: 200 mg; ID 1502−1513: 400 mg; ID 1604−1610: 600 mg; ID 1701−1713: 800 mg

Multiple ascending dose groups: ID 2301−2311: 100 mg; ID 2402−2418: 200 mg; ID 2505−2513: 400 mg

OCC=1: Day 1; OCC=3: Day 7 of multiple ascending dose study.

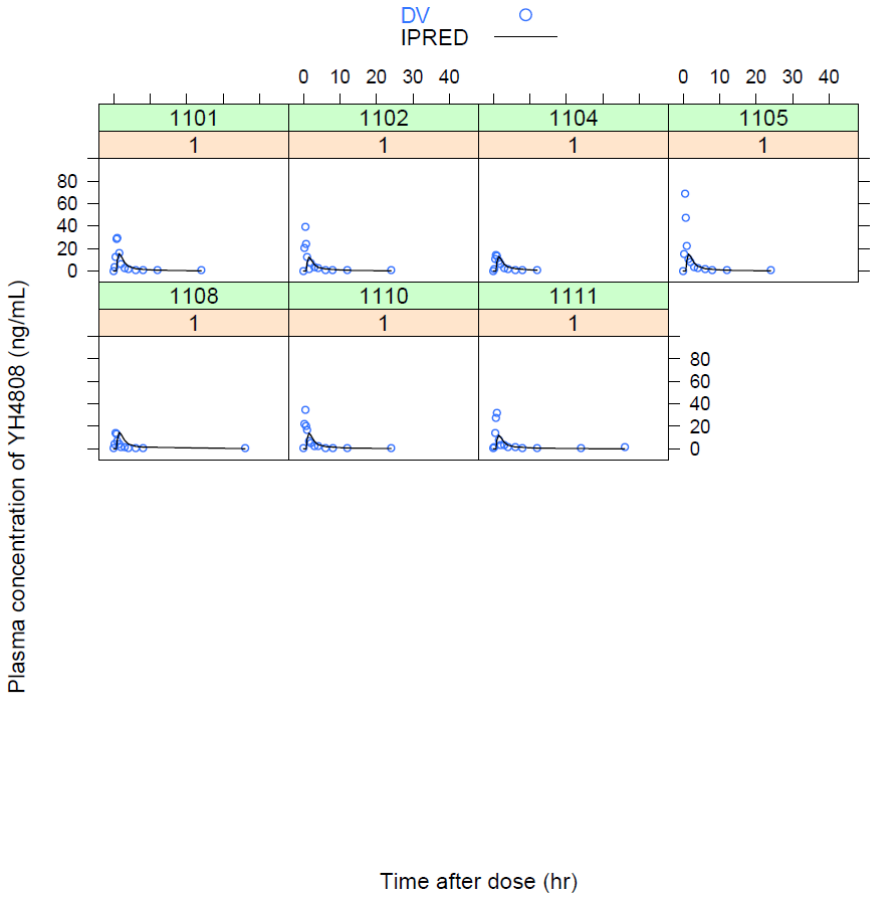

Individual fitting plots for the final pharmacokinetic and pharmacodynamic model of YH4808 (DV: dependent variable, IPRED: individual predicted values) (continued)

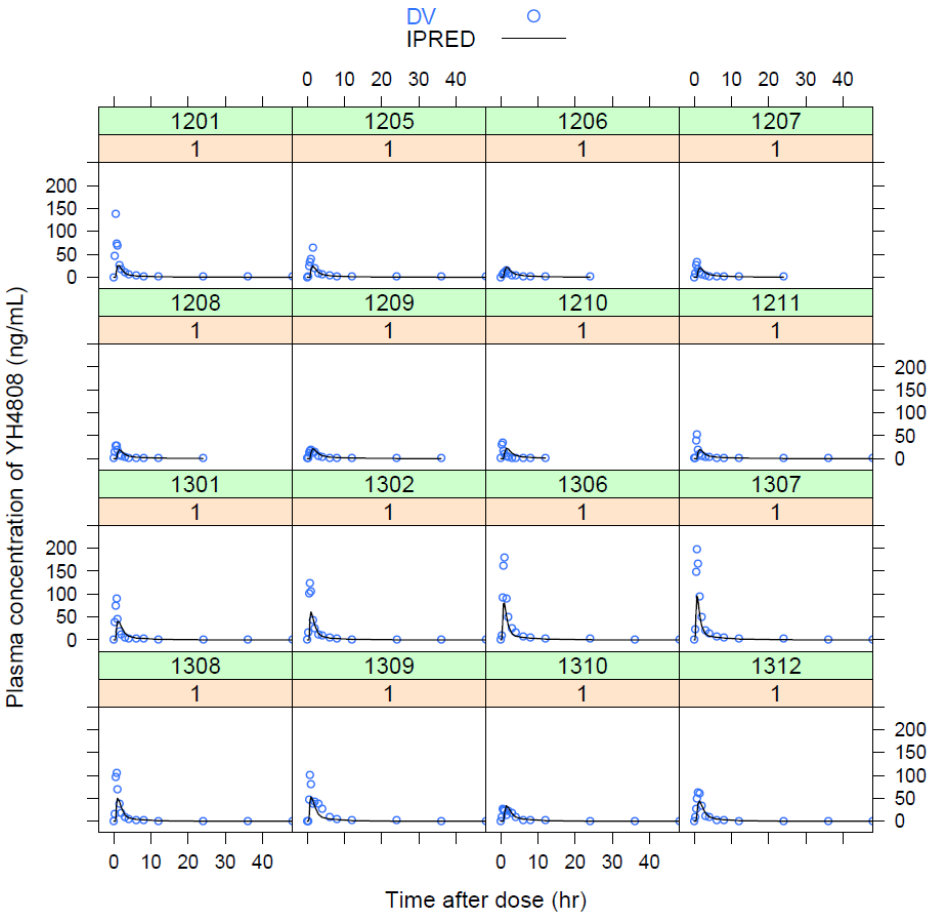

Individual fitting plots for the final pharmacokinetic and pharmacodynamic model of YH4808 (DV: dependent variable, IPRED: individual predicted values) (continued)

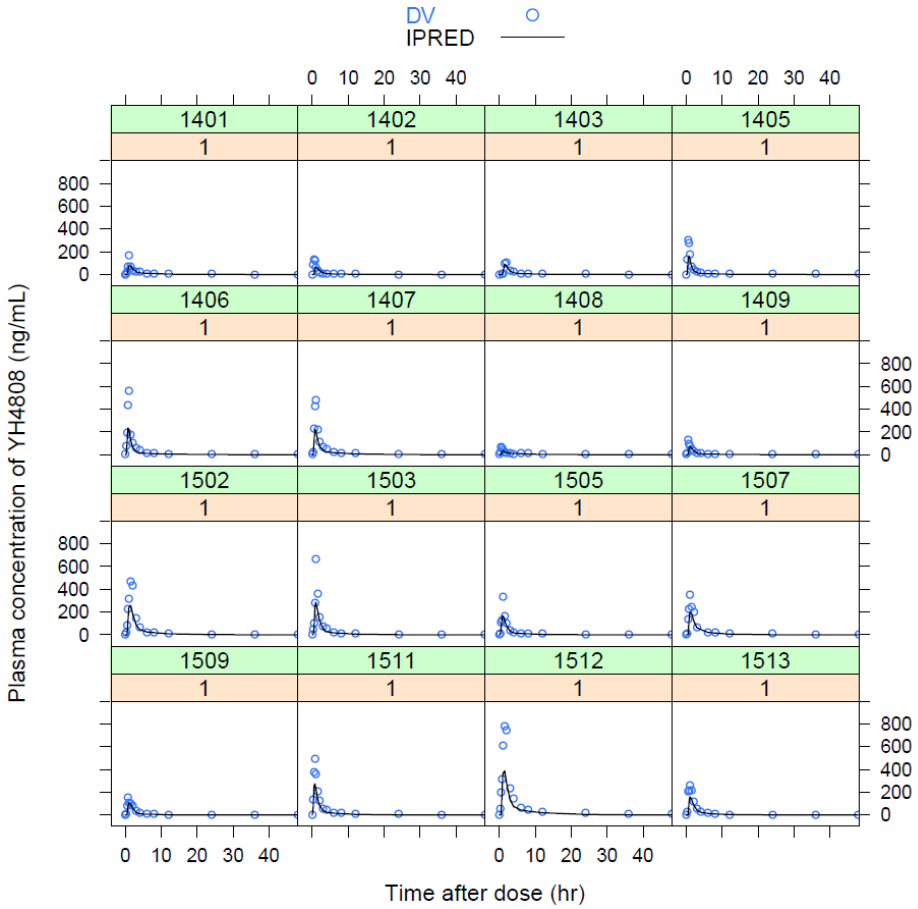

Individual fitting plots for the final pharmacokinetic and pharmacodynamic model of YH4808 (DV: dependent variable, IPRED: individual predicted values) (continued)

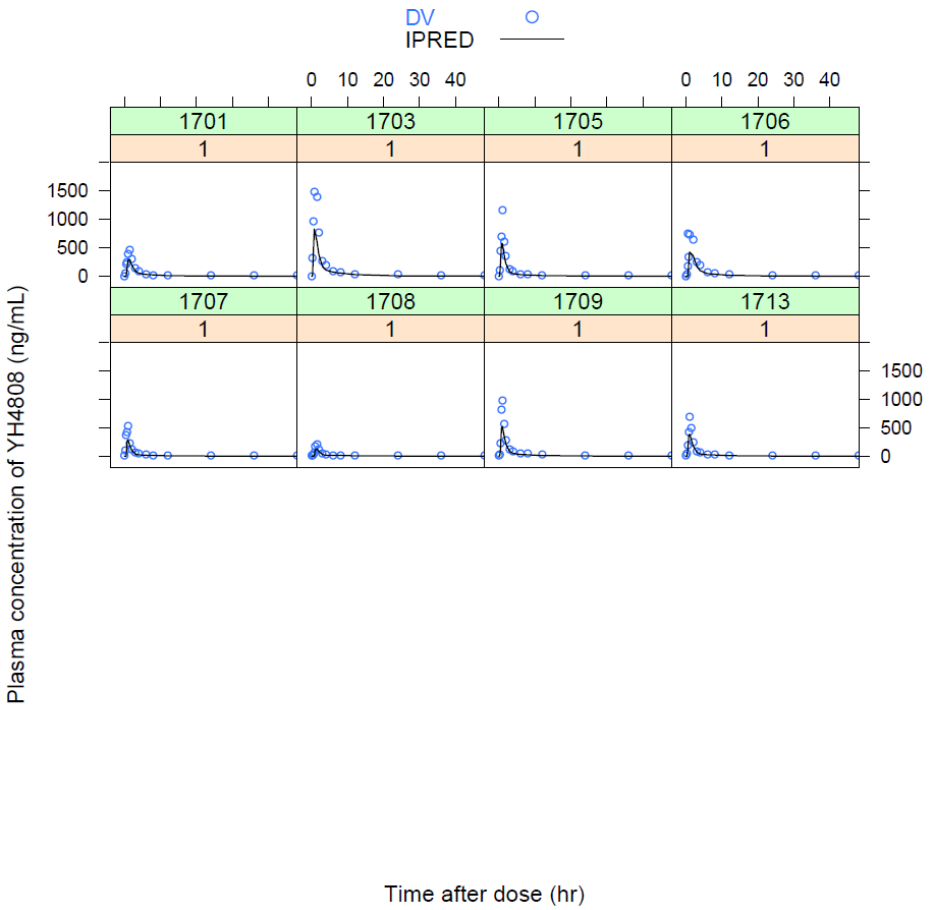

Individual fitting plots for the final pharmacokinetic and pharmacodynamic model of YH4808 (DV: dependent variable, IPRED: individual predicted values) (continued)

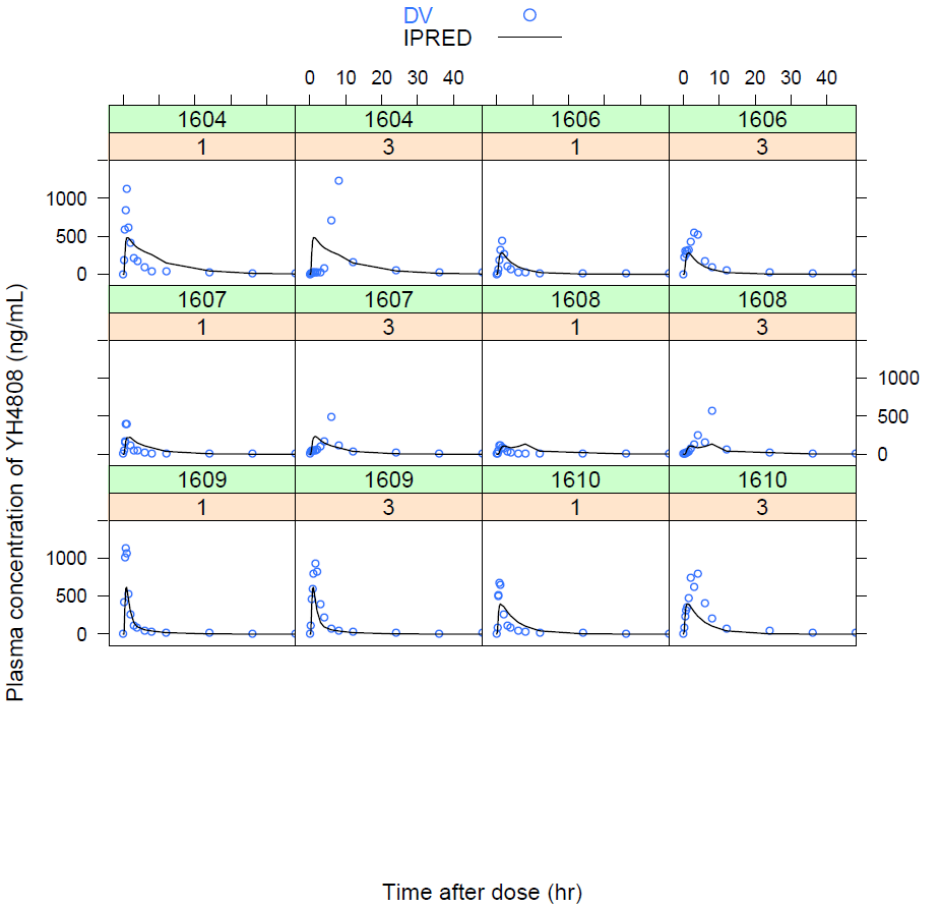

Individual fitting plots for the final pharmacokinetic and pharmacodynamic model of YH4808 (DV: dependent variable, IPRED: individual predicted values) (continued)

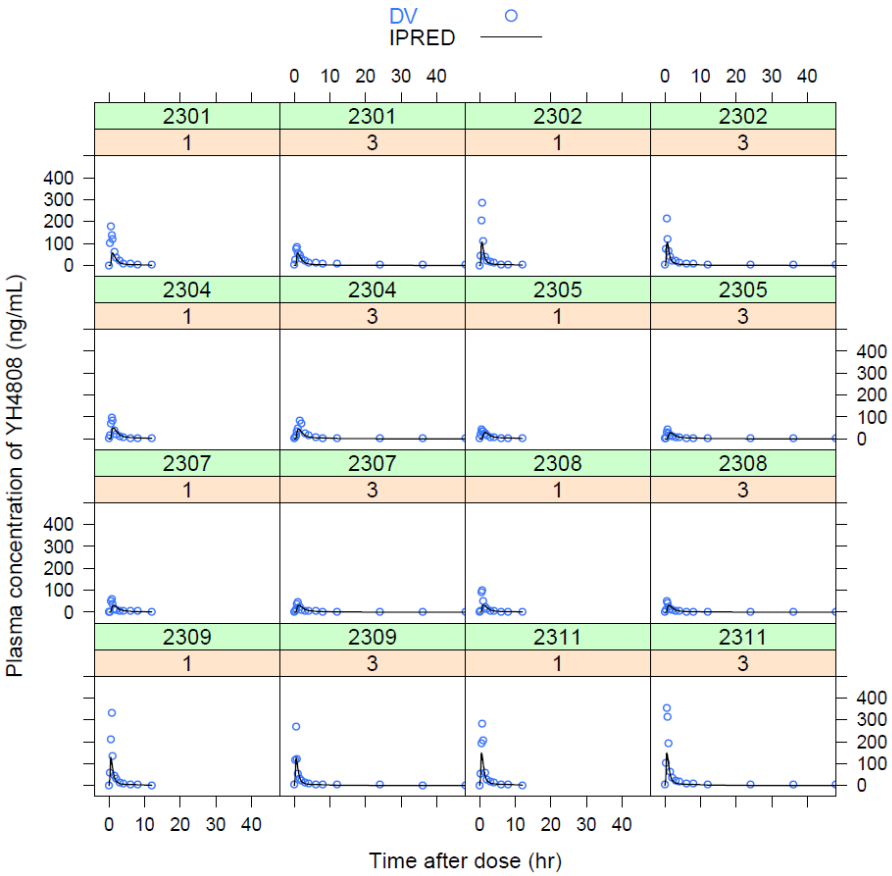

Individual fitting plots for the final pharmacokinetic and pharmacodynamic model of YH4808 (DV: dependent variable, IPRED: individual predicted values) (continued)

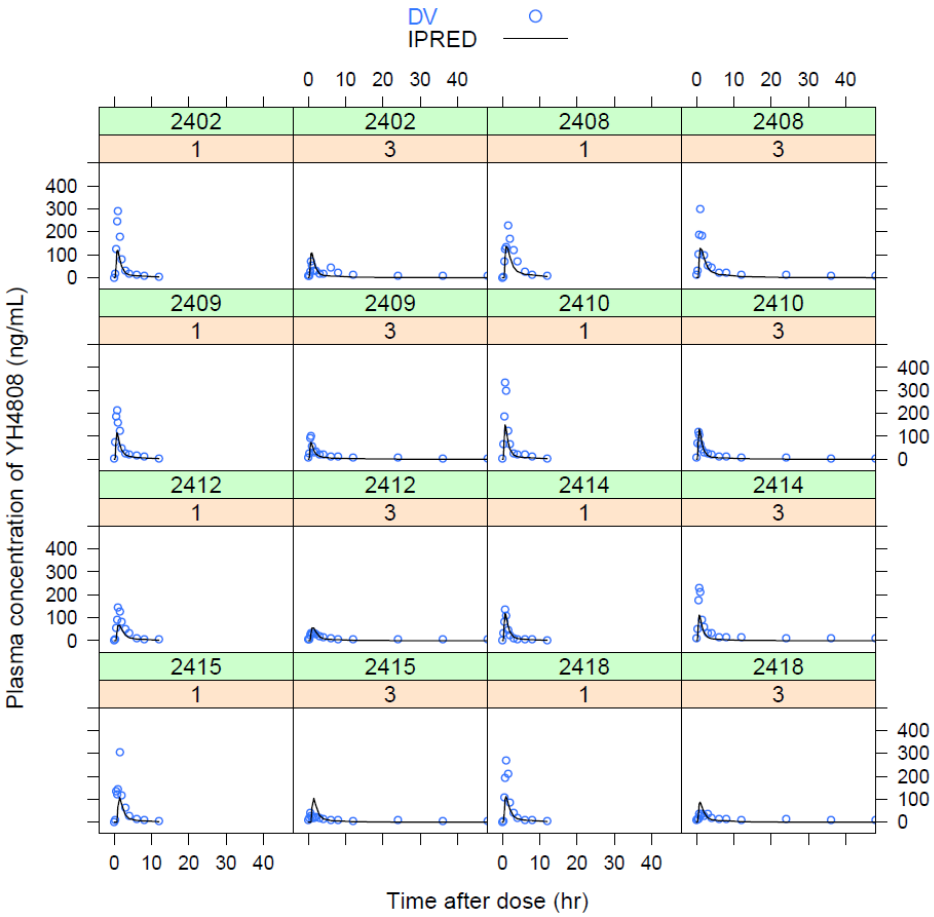

Individual fitting plots for the final pharmacokinetic and pharmacodynamic model of YH4808 (DV: dependent variable, IPRED: individual predicted values) (continued)

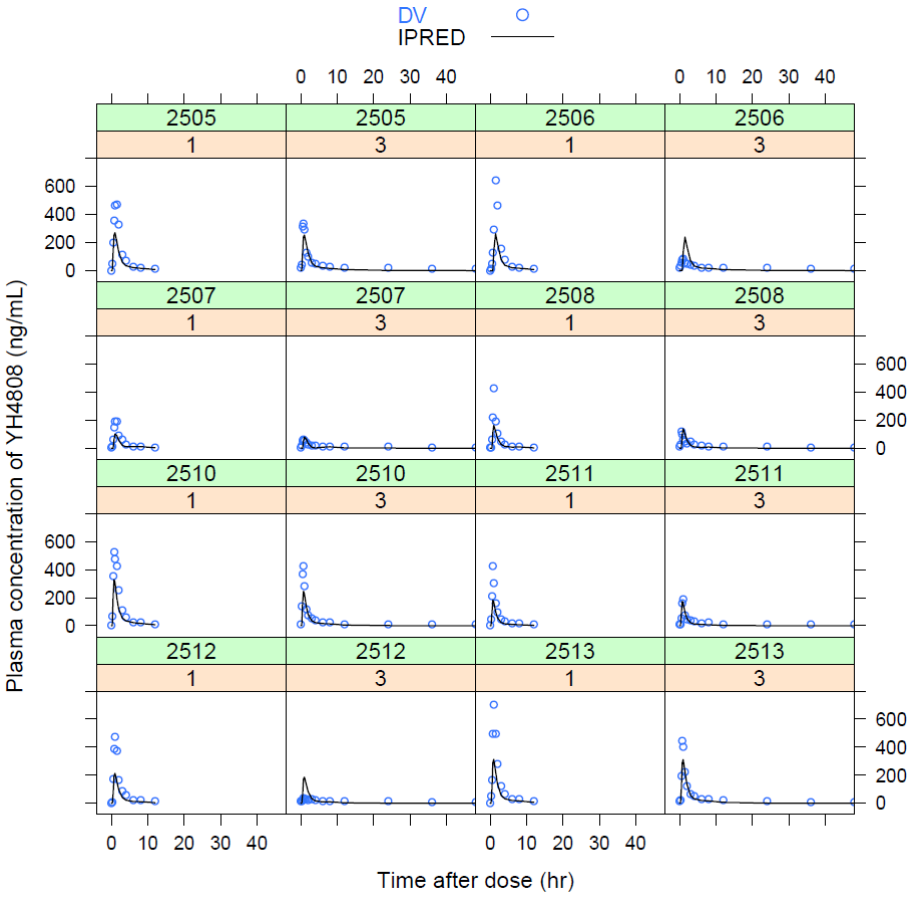

Individual fitting plots for the final pharmacokinetic and pharmacodynamic model of YH4808 (DV: dependent variable, IPRED: individual predicted values) (continued)

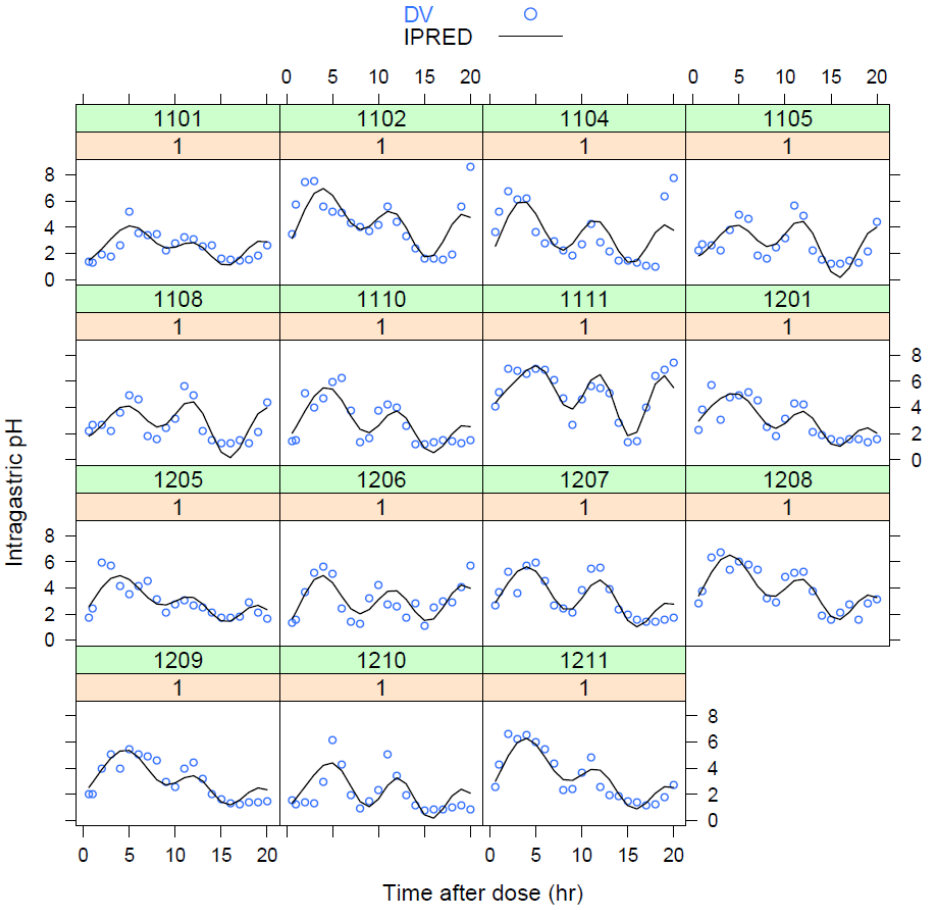

Individual fitting plots for the final pharmacokinetic and pharmacodynamic model of YH4808 (DV: dependent variable, IPRED: individual predicted values) (continued)

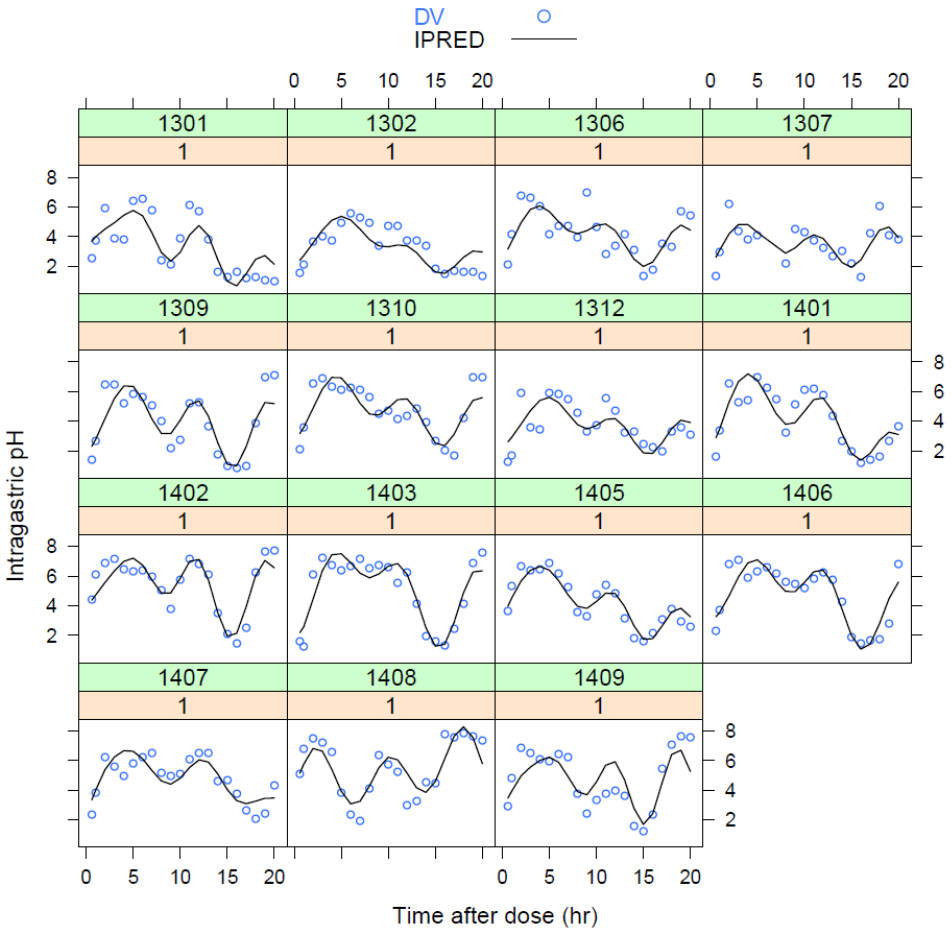

Individual fitting plots for the final pharmacokinetic and pharmacodynamic model of YH4808 (DV: dependent variable, IPRED: individual predicted values) (continued)

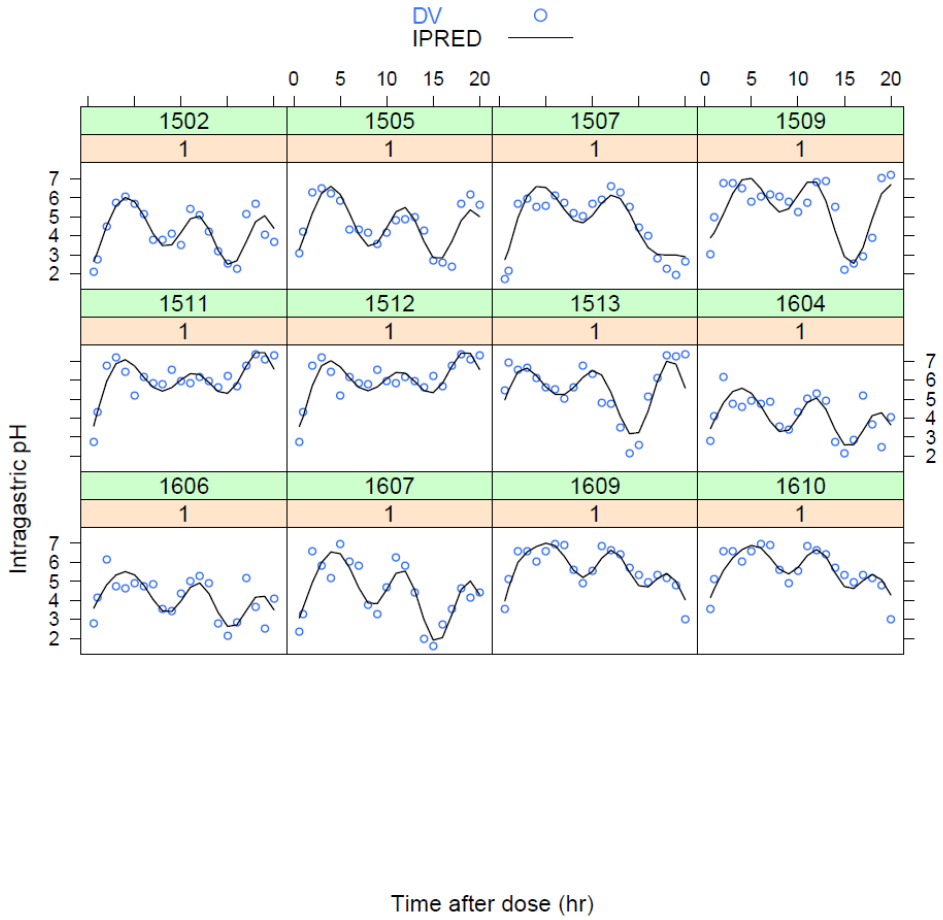

Individual fitting plots for the final pharmacokinetic and pharmacodynamic model of YH4808 (DV: dependent variable, IPRED: individual predicted values) (continued)

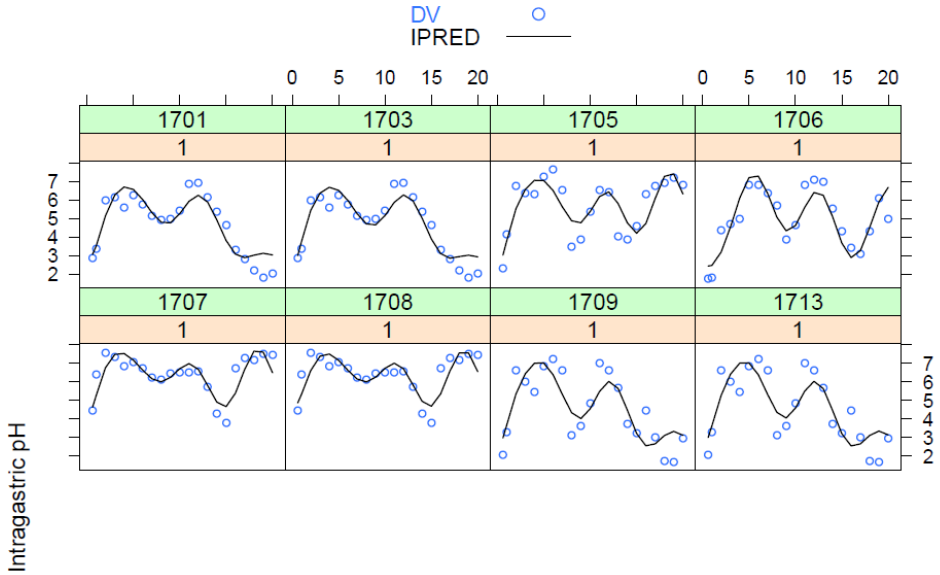

Individual fitting plots for the final pharmacokinetic and pharmacodynamic model of YH4808 (DV: dependent variable, IPRED: individual predicted values) (continued)

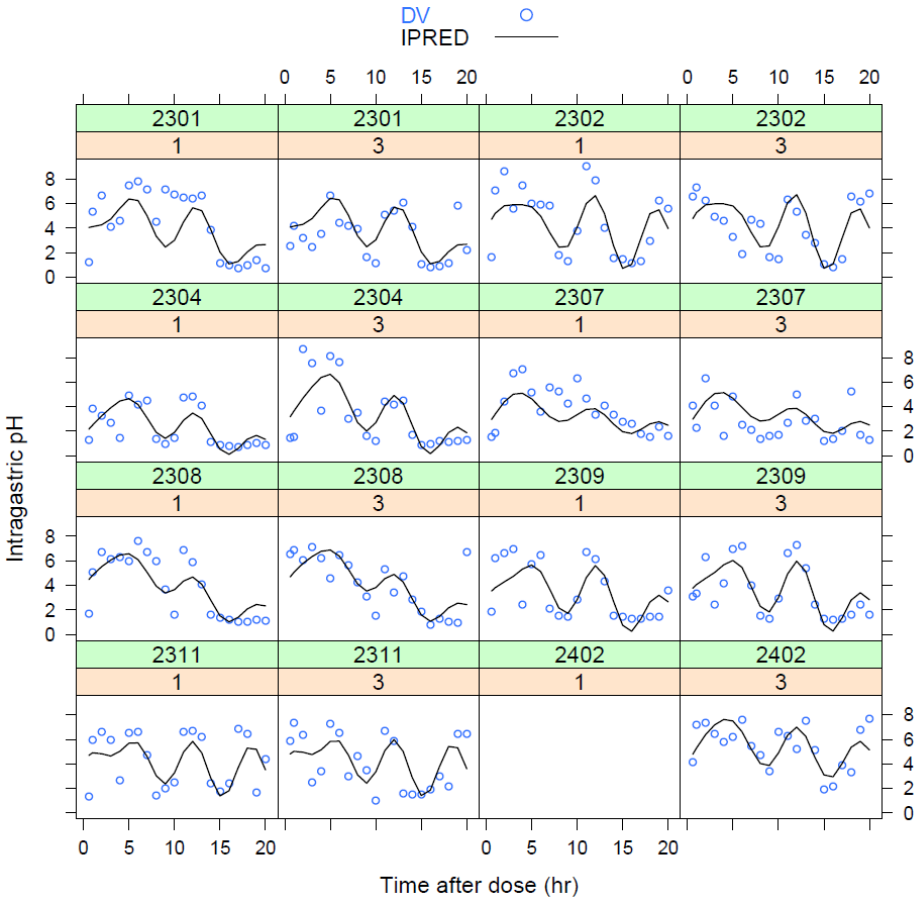

Individual fitting plots for the final pharmacokinetic and pharmacodynamic model of YH4808 (DV: dependent variable, IPRED: individual predicted values) (continued)

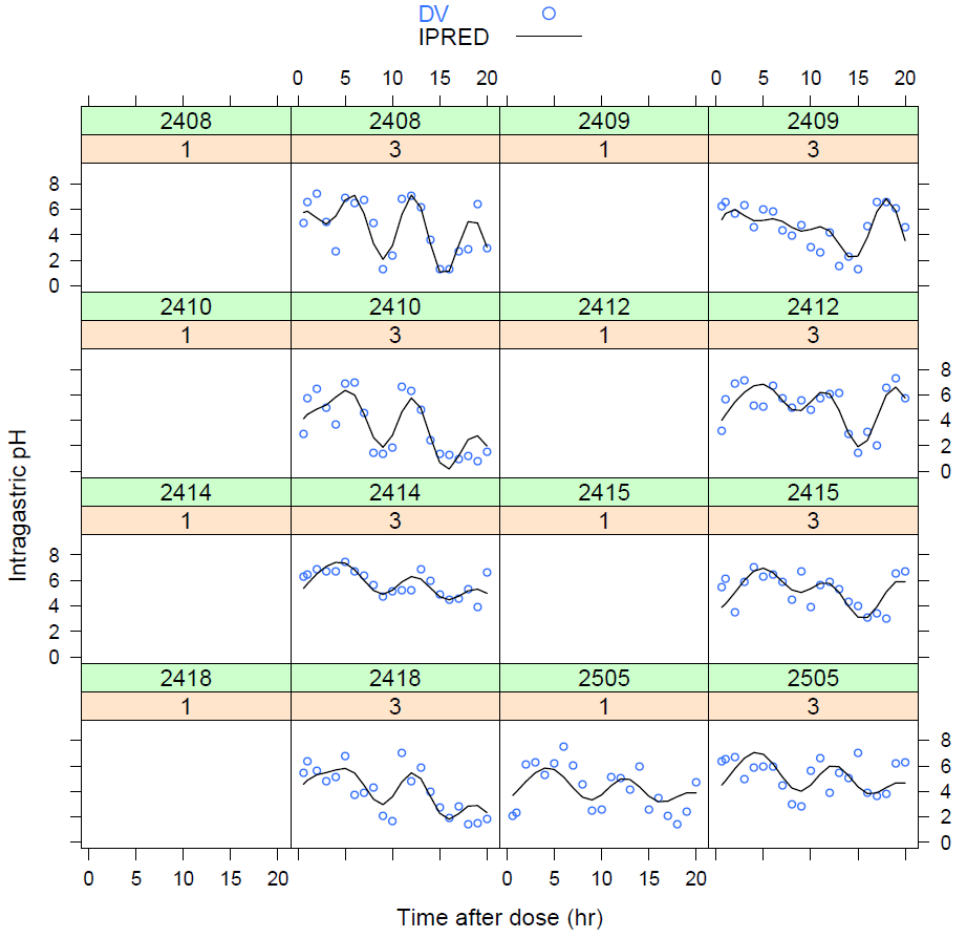

Individual fitting plots for the final pharmacokinetic and pharmacodynamic model of YH4808 (DV: dependent variable, IPRED: individual predicted values) (continued)

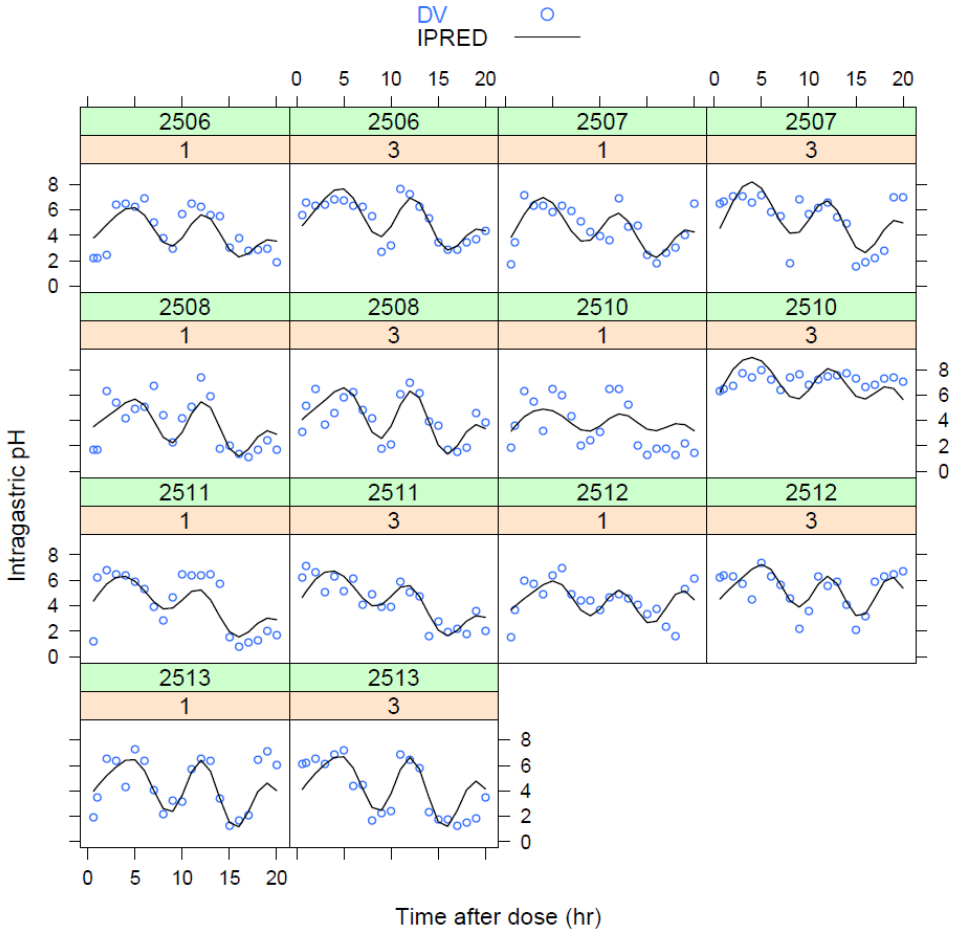

4. NONMEM control stream of the final PK and PD model

```
$SUBROUTINE ADVAN13 TOL=6

$MODEL    COMP=(DEPOT) COMP=(CENTRAL) COMP=(PERIPH)
COMP=(EFFECT)

$PK

CL = THETA(1)*EXP(ETA(1))*(WT/70)**THETA(24)

V2 = THETA(2)*EXP(ETA(2))

Q = THETA(3)*EXP(ETA(3))

V3 = THETA(4)*EXP(ETA(4))

KA = THETA(5)*EXP(ETA(5))

ALAG1 = THETA(6)*EXP(ETA(6))



K20 = CL/V2

K23 = Q/V2

K32 = Q/V3

K12 = KA

IF (CMT .EQ. 2) THEN

S2 = V2


ELSE

S2 = 1

ENDIF


A0 = THETA(7) ;* EXP(ETA(7))

A1 = THETA(8) ;* EXP(ETA(8))

A2 = THETA(9) ;* EXP(ETA(9))

A3 = THETA(10) ;* EXP(ETA(10))

A4 = THETA(11) ;* EXP(ETA(11))

C1 = THETA(12) ;* EXP(ETA(12))

C2 = THETA(13) ;* EXP(ETA(13))

C3 = THETA(14) ;* EXP(ETA(14))

C4 = THETA(15) ;* EXP(ETA(15))
```

```
E0 = A0 + A1*COS(2*3.1416*(TAD-C1)/24) + A2*SIN(2*3.1416*(TAD-C2)/18) + A3*COS(2*3.1416*(TAD-C3)/12) + A4*SIN(2*3.1416*(TAD-C4)/6)


EMAX = THETA(16)*EXP(ETA(7))

EC50 = THETA(17)*EXP(ETA(8))

KE0 = THETA(18)*EXP(ETA(9))

EDMAX = THETA(19)*EXP(ETA(10))

ED50 = THETA(20)*EXP(ETA(11))


$DES

DCP = A(2)/V2

DCE = A(4)


DADT(1) = -KA*A(1)

DADT(2) = -K23*A(2)-K20*A(2)+K32*A(3)+KA*A(1)

DADT(3) = -K32*A(3)+K23*A(2)

DADT(4) = KE0*(DCP-DCE)


$ERROR

CP = A(2)/V2

CE = A(4)

Q1 = 1 ; dummy indicator for compartment 2


IF (CMT .EQ. 4) Q1=0


PH = E0*(1+(EMAX*CE)/(EC50+CE)) ; Emax model for pH driven by effect compartment concentration

PHPK = 1-(EDMAX*PH)/(ED50+PH) ; Inhibitory effect model for the feedback by pH for plasma concentration of YH4808

IPRED = Q1*CP*PHPK + (1-Q1)*PH

W = Q1*SQRT(THETA(21)**2*IPRED**2 + THETA(22)**2) + (1-Q1)*SQRT(THETA(23)**2)

IRES = DV-IPRED

IWRES = IRES/W

Y = IPRED+W*EPS(1)


$THETA (0,500) ; CL

 (0,500) ; V2
```

```
(0,500) ; Q

(0,5000) ; V3

(0,1) ; KA

(0,0.1) ; ALAG1

(0.1,5) ; A0

(0.1,1) ; A1

(0.001,1) ; A2

(-1,0.1) ; A3

(-1,0.1) ; A4

(0.1,10) ; C1

(0.01,1) ; C2

(0.01,1) ; C3

(0.1,5) ; C4

(0,0.1) ; EMAX

(0,500) ; EC50

(0.01,1) ; KE0

(0,0.5) ; EDMAX

(0,5) ; ED50

(0,0.3) ; Prop RE (sd)

0.01 FIX

(0,0.5) ; Additive RE

(0,1) ; power term of weight

$OMEGA  0.5  ;        ETA1

 0.5  ;        ETA2

 0.5  ;        ETA3

 0.5  ;        ETA4

 0.5  ;        ETA5

 0.5  ;        ETA6

 0.5  ;        ETA7

 0.5  ;        ETA8

 0.5  ;        ETA9

 0.5  ;       ETA10

 0.5  ;       ETA11

$SIGMA  1.0  FIX

$ESTIMATION METHOD=1 INTER MAXEVAL=9999 NOABORT
SIGL=6 NSIG=2 PRINT=5 POSTHOC

$COVARIANCE
```

```
$TABLE       ID TIME TAD OCC AMT CMT MDV IPRED IWRES
CWRES ONEHEADER NOPRINT FILE=sdtab1007

$TABLE       ID CL V2 Q V3 ALAG1 KA E0 EMAX EC50 KE0
EDMAX ED50 FIRSTONLY ONEHEADER NOPRINT NOAPPEND
FILE=patab1007
```

국문 초록

위산 펌프 길항제와 위 내 산도 상호간의 효능 관계를 규명하기 위한 생리학적 약물 동태 모델과 약동/약력학 모델 구축 연구

-칼륨 경쟁적 위산 분비 억제제인 YH4808 을 예시로-

이현아

방사선융합의생명 전공

서울대학교 융합과학기술대학원

서론: 위산 분비와 관련된 질환의 치료제로 개발 진행 중인 YH4808 은 위산 분비를 담당하는 효소인 H+/K+-ATPase 에 작용하여, 이 효소를 가역적, 선택적으로 불활성화시키는 칼륨 경쟁적 위산 분비 차단제 (Potassium-Competitive Acid Blocker, P-CAB)이다. 임상 1 상 시험 결과, YH4808 30-800 mg 을 건강한 남성 자원자에게 단회 투여하였을 때, YH4808 의 약동학(혈중 농도 변화)은 용량 비례적인 양상을 보였다. 그러나, YH4808 반복 투여 시(특히, 고용량군 (200, 400 mg)), 전신 노출이 감소하였다. YH4808 반복 투여 후, 위 내 pH 상승에 의한 YH4808 의 용해도 감소가 노출 감소의 주요 원인으로 제기되었다.

본 연구에서는, 첫째, 단회 및 반복 투여 시 YH4808 의 약동학(혈중 농도) 프로파일을 예측하기 위한 생리학적 약물 동태 모델을 구축하였고, 이 모델을 사용하여 고용량 반복 투여 시 나타나는 YH4808 의 노출 감소를 기전 중심으로 원인을 규명하였다. 둘째로, YH4808 단회 및 반복 투여 후, YH4808 의 혈중 농도와 시간에 따른 위 내 pH 변화와의 상호 관계를 정량적으로 평가하기 위하여 약동/약력학 모델을 구축하였다.

방법: 생리학적 약물 동태 모델은 YH4808 의 물리화학적 특성, *in vitro* 비임상 데이터, 임상 데이터를 사용하여 개발된 후, 임상 1 상 단회 투여 데이터를 사용하여 개선되었다. 생리학적 약물 동태 모델 구축에는 SimCYP (Certara USA, Inc., Princeton, USA) 시뮬레이터가 사용되었다. 생리학적 약물 동태 모델의 각 구획은 뇌, 심장, 폐, 신장, 근육, 비장, 간, 위장관, 췌장을 의미하고, 그 외 나머지 조직들은 하나의 구획으로 만들었다. 위장관과 간을 제외한 모든 구획은 약물 분포가 매우 신속하게 일어나고, 약물의 청소율은 혈류에 의해서 제한된다고 가정하였다. YH4808 의 체내 흡수 양상의 경우, 위장관과 간에서는 permeability−limited disposition 을 가정하고, SimCYP 시뮬레이터에 내장되어 있는 the advanced dissolution, absorption and metabolism (ADAM) 모델을 사용하여 예측하였다. YH4808 은 대부분 담즙으로 배설되므로, 청소율은 *in vitro* hepatic microsomal intrinsic

clearance data 를 이용하여 계산하였다. 약동/약력학 모델은 YH4808 의 임상 1 상 시험을 완료한 건강한 자원자 (단회 (30-800 mg) 또는 반복 (100-400 mg) 투여)의 혈중 농도와 위 내 pH 데이터 (위약 데이터 포함)를 하나의 데이터셋으로 합쳐 동시적으로 개발하였다. 약동/약력학 파라미터의 추정은 NONMEM (version 7.3., ICON Development Solutions, Ellicott City, MD, USA) 프로그램에 내장되어 있는 first-order conditional estimation with interaction (FOCE-I) 방법을 사용하였고, 공변량 (예., 나이, 체중, 키)의 영향 또한 평가하였다. 추정된 파라미터의 정밀도, diagnostic plot, visual predictive checks plot 결과 등을 고려하여 최종적으로 가장 적합한 모델을 선정하였다.

결과: 생리학적 약물 동태 모델 구축 연구 결과, 단회 투여의 경우 개선된 모델을 사용하여 YH4808 의 혈중 농도 양상이 잘 예측된 반면, 반복 투여의 경우 200 mg 과 400 mg 용량군에서 나타난 약물의 노출 감소 현상은 잘 예측하지 못하였다. YH4808 반복 투여시 고용량 군에서 나타나는 이런 약물의 노출 감소 현상의 원인을 찾기 위하여 위 내 pH 증가가 YH4808 의 용해도를 감소시키고, 이런 약물의 물리화학적 특성이 약물 노출을 감소시킨다고 가정하였다. 이러한 가정은 구축된 생리학적 약물 동태 모델에서 위 내 pH 를 인위적으로 상승시킴에 따른

YH4808 의 체내 노출 변화를 시뮬레이션하여 최종적으로 검증하였다.

다음으로, 약동/약력학 모델 구축 연구 결과, 흡수 지연 시간이 있는 1 차 흡수를 보이는 2 차 구획 약동학 모델과 효과처 구획 모델이 연결된 S 자 모양 최대 효과 모델 (sigmoid maximum effect model)을 사용하여 YH4808 투여 후 관찰된 혈중 농도와 24 시간 동안의 위 내 pH 프로파일을 잘 예측하였다. 또한, 시간에 따른 위 내 pH 변화가 다시 YH4808 혈중 농도에 영향을 주는 현상을 설명하기 위하여, 위 내 pH 상승이 YH4808 의 상대적 생체이용률을 감소시키는 되먹임 경로를 모델에 추가하였다.

결론: 본 연구에서, 생리학적 약물 동태 모델은 YH4808 단회 및 반복 투여 후 YH4808 의 혈중 농도를 잘 예측하였고, 구축된 모델을 사용하여 YH4808 의 pH 의존 용해도(pH−dependent solubility)가 반복투여 시 나타나는 노출 감소 현상의 원인이라는 것을 증명하였다. 이러한 기전을 YH4808 의 약동/약력학 모델에 반영하여 단회 및 반복 투여 시 YH4808 의 혈중 농도와 위 내 pH 변화와의 상호 관계를 정량적으로 잘 설명하였다. 결론적으로, 본 연구는 YH4808 의 체내 노출과 위 내 pH 변화 간의 관계를 파악하는데 기전적 통찰력을 제공하였고, 이는 YH4808 의 최적 용량 용법을 제시하는데 기여할 수 있을 것이다.

주요어: 위 내 pH, 생리학적 약물 동태, 약동학, 약력학, 모델링, 시뮬레이션, 칼륨 경쟁적 위산 분비 차단제

학 번: 2015-30724

ACKNOWLEDGEMENTS

Firstly, I would like to express my sincere gratitude to my supervisor Prof. Howard Lee for the continuous support of my research, for his patience, motivation, and immense knowledge. His guidance helped me in all the time of research and writing of this thesis.

Besides my supervisor, I would like to thank the rest of my thesis committee: Prof. Sung-Joon Ye, Prof. Kyung-Sang Yu, Prof. Jung Mi Oh, and Dr. Kyeong-Ryoon Lee, for their insightful comments and encouragement.

I wish to thank my fellow labmates of CCADD, Dr, Jeong-An Gim, Yoomin Jeon, Siun Kim, Tae Kyu Chung, and Jung-Chun Gwon, for helping me during these years of hard work and for being such good friends, inside and outside the lab.

Last but not the least, I would like to thank my parents, Seok Joon Lee and Pil Ja Moon, whose love and guidance are with me in whatever I pursue. They are the ultimate role models. I am grateful to my mother-in-law and my sister for all of the sacrifices. Most importantly, I wish to thank my loving and supportive husband, Youngmin Lee, and my precious child, Seungbin Lee, who provide unending inspiration.